Ljubinko B. Kevac[1] and Mirjana M. Filipovic[2]

DEVELOPMENT OF CABLE-SUSPENDED PARALLEL ROBOT, CPR SYSTEM, AND ITS SUB-SYSTEMS

Abstract. This paper is an overview of the modeling approaches of different constructions of Cable Suspended Parallel Robots, CPR systems. Each new design requires studious approach and detection of specific phenomena, which needs to be defined through the process of mathematics modeling. The characteristic features of CPR structures can be grouped as follows: 1. shape of the work space (plane, spatial), 2. number of motors, 3. type of motors, translational or rotational motors, 4. number of hanging points, 5. total number of ropes for the functional work of the CPR system, 6. number of ropes from the camera carrier to the hanging points, 7. type of cable winding/unwinding system, CWU system, and influence of new dynamic variables: winch radius of CWU system and cable length on dynamic response of CWU system and finally on dynamic response of CPR system. Each of these characteristics differently affects the response of the CPR system. The geometric relations between the motor and the camera carrier motion are very important for the modeling of the system. The mathematical model (kinematic and dynamic) is defined as generally solution. It is evident that the choice of construction of CPR significantly affects the response of this system. The validity of the obtained theoretical contribution has been illustrated through several case studies by using a newly developed software packages.

Mathematics Subject Classification (2010): Primary: 70-99, 74-99, 70F35, 92C10, 74L10; Secondary: 70Exx, 70KXX, 74M05, 37H20.

Keywords: mathematics modeling, cable suspended parallel robots, cable winding/unwinding system.

[1] School of Electrical Engineering, The University of Belgrade, Serbia
ljubinko.kevac@gmail.com
[2] Mihailo Pupin Institute, University of Belgrade, Serbia
mirjana.filipovic@pupin.rs

Contents

1. Introduction

The systems for observation of the workspace with moving objects have been developed and analyzed worldwide in various research areas and for different purposes. It is important that both kinematic and dynamic modeling of these systems is considered. Relatively new systems that are designed and considered are parallel systems. In paper [1], the design of a planar three-degree-of- freedom parallel manipulator is considered from a kinematic viewpoint. The paper [2] presents the first and second order kinematic analysis of a three-degree-of- freedom 3-RPS parallel robot mechanism. In paper [3] authors present algorithms that enable precise trajectory control of NIMS3D, an under constrained, three-dimensional cabled robot intended for use in actuated sensing. In paper [4] author presents several prototypes of wire-driven parallel robots, recently designed and which use two different actuation schemes. The wrench-closure workspace of parallel cable-driven mechanisms is the set poses of their mobile platform for which the cables can balance any external wrench in [5]. Parallel cable-driven Stewart-Gough platforms consist of an end-effector which is connected to the machine frame by motor driven cables in [6]. The paper [7] presents the recent results from a newly designed parallel wire robot which is currently under construction. Firstly, an overview of the system architecture is given and technically relevant requirements for the realization are identified. The paper [8] presents an auto-calibration method for over constrained cable-driven parallel robots using internal position sensors located in the motors. Wire-driven parallel robot has attracted the interest of researchers since the very beginning of the study of parallel robots [9].

In the current literature survey there is no any mathematical model of the cable-suspended-parallel robots with double parallel ropes and there is no available procedure for generating the Jacobian matrix of the similar systems. Another problem is that the current published models do not include the motors dynamics. The analysis and synthesis of these complex systems cannot be proper without the motor dynamics, because it represents the dominant dynamics for any electro mechanical system.

The kinematic formulation of the presented CPR system is a key contribution in this paper, which will be used for the system realization. This formulation can be used for determining the Jacobian matrix of any CPR system configuration. This methodology for developing the kinematic model of selected CPR systems is named the KinCPR-Solver (Kinematic Cable Parallel Robot Solver), and it gives a precise direct and inverse kinematic solutions.

The dynamic model is generated using the fundamental dynamic theory based on the Lagrange's principle of virtual work which for most CPR systems was not directly applied because of the systems complexity. The Lagrange's principle of virtual work has been used for solving the complex relation between the resultant motor load moment (acting as a load at the motor shaft) and external forces (acting at the camera carrier). The Lagrange 's principle of virtual work can be directly applied to original form to the RSCPR system, as in paper [10], which has one rope from camera carrier to the pivot point of the system. There can be several reasons for the adaptation of Lagrange's principle of virtual work as presented in paper [11]. First of them is presence of two parallel ropes in any direction and (or) second is when the motor winds or unwinds two ropes at the same time about the coil. In the RFCPR as in paper [11], CPR-A [12], CPR-B, CPR-C [13], and CPR-D [14] systems, the adapted Lagrange's principle of virtual work can provide the correct relation between the internal and external forces. The resulting equation developed by the Lagrange's principle of virtual work has been used for determining the motors dynamic model of the CPR system.

The mathematical model of the motors is determined using the Lagrange's equations second order and expressed with the generalized coordinates.

In this paper the camera carrier workspace has the shape of a parallelepiped, such that the camera carrier hangs over the ropes properly connected on the four highest points i.e. the four upper angles of the workspace. The suspension system is defined in these four points.

A camera workspace is an area where the camera can move quietly and continuously by following the observed object.

A camera carrier moves freely in the 3D space which enables the recording of the object from the above.

This gives a unique feeling to the viewer to follow the event easy from an unusual proximity and to be very close to the action regardless of the size of the observed space.

The CPR, like many robotic systems is very complex and includes many sub-systems, which interact with each other, compatibility conditions of displacement and kinetic parameters of the system dynamics.

A new procedure for creating the reference trajectory of the CPR system's camera intended for object tracking and monitoring in real time is presented in [15]. This procedure is named the CPR Trajectory Solver. We started with a presumption that the CPR system's camera needs to follow an object which is moving within the camera's sight at the lowest plane of the camera's workspace. The CPR Trajectory Solver has continuous information about the position and orientation of the camera during the task execution.

The paper [16] contains two contributions. The first one is the idea for application of the CPR system intended for monitoring and treating the plants in green-houses. The second contribution is a theoretical one. We have identified and defined the problem of deviation of camera and diffuser carrier's position and orientation during its motion. The carrier's hanging point and center of mass do not overlap in its workspace, which was an idealized presumption in the previously published works.

Main contribution of work [17] is development of novel methodology for choosing actuator for a CPR-8 system, named CPR-ACM. This methodology implies the formulation and application of a data base which contains catalogue parameters of the actuators available at the market. Both, user and designer define together the parameters and desired feasible workspace of the CPR-8 system being designed. The methodology is illustrated by a logic flow chart.

In paper [18], multivariable procedure for choosing the parameters of CPR system was developed. This was performed because of the need for the load carrier to move in broader area of its geometric workspace, i.e. for achieving its feasible workspace. Given task is defined by: configuration of the system, its dimensions, weight of the load, load's velocity; while the parameters which are set to achieve this goal are: type of the winch and its winding/unwinding radius, gearbox characteristics, and especially characteristics of the motor. This paper points out another important fact that task of choosing a motor is not solved by only choosing motor by its nominal output power. Results presented in this paper show that motor with power of 140 W gives better results than motor with nominal power of 420 W.

CPR systems are also used for implementation of humanoid robotic systems. By thorough analysis of the CPRAM system, it can be seen that well-known mathematical models of these systems have generated instability and oscillatory behavior around the horizontal position of artificial muscle of the forearm. The main contribution and novelty of the paper [19] is new, original form of mathematical model of the forearm artificial muscle. To define kinematic and dynamic models of this system, its thorough analysis was needed. With this analysis, system's geometry and characteristic relations were defined. Geometry of the CPRAM system reveals and defines new, not yet recognized geometric relations of the artificial forearm.

Various complex mechatronic systems have cables (ropes as well) winding/unwinding systems as main sub-systems. Authors of papers [10-19] dealt with design, analysis and synthesis of the cable suspended parallel robotic system (CPR system). They have used a well-known winding/unwinding sub-system presented in [20].

There are a lot of similar systems in different areas of science and engineering. Some of these systems are: measuring mechanism, machines in textile industry, cable logging systems in civil engineering and forestry, cranes, systems in ship-ping industry, CPR (Cable-suspended Parallel Robot) and other complex cable driven systems.

Phenomenon of cable winding/unwinding (hereinafter referred to as: CWU system) on winch is present in different applications, so in this paper the importance of its analysis will be emphasized. Some of papers which have inspired the research presented in this paper will be mentioned in the following paragraphs.

Authors of [21] have written a review paper on application of cable logging systems. Goals of [21] are far-reaching because authors define the instruction set for users that use those systems. These instructions help the users to solve several problems such are protection of workers, soil and forests. The author of [22] gives a detailed image about the history of CWU systems. The author points the fact that these systems were used in different areas for several millennia. One type of systems which use CWU sub-systems are cranes and these systems are thoroughly analysed in [23].

In [23-25], authors present theoretical and experimental contribution to analysis and synthesis of kinematics and dynamics of winding/unwinding process of thread from a balloon. Fluctuating tensions in a perfectly flexible string unwinding from a stationary package were considered in [24]. Also, dependence of unwinding tensions on air resistance, unwinding speed, angle of winding on the package etc. was examined. Based on results from [24], in [25] over-end unwinding of yarn from a stationary helically wound cylindrical package was considered. An improved theory for the variation of yarn tension during high speed over-end unwinding from cylindrical yarn packages based upon the theory of bent and twisted elastic rods was presented in [26]. Authors of [27] presented a dynamic simulation for wire cable on the tower crane. They have considered not only the contact with the winch drum, but also the characteristics of the hydraulic system using SINDYS. Specifically, the following points have been demonstrated: 1. The contact between the winch drum and wire cable can be modelled by using the variable-length truss elements and the contact spring. 2. The dynamic behavior of wire cable that occurs at hydraulic winch stopping is affected by the dynamic characteristics of the hydraulic sys-tem. 3. A slow-stopping hydraulic winch system has been proposed, and the sys-tem can prevent disordered winding even if the winch is rapidly operated.

In [28], authors presented the mathematical model of a pipelay spread. In the model, elasto-plastic deflections of the pipe, its large deformations and contact problems were considered. The modification of the rigid finite element method was used to discretize the pipe.

Wire-guided control technologies are widely used to increase the targeting accuracy of advanced military weapons through the use of unwinding dispensers to guarantee that unwinding occurs without any problems, such as tangling or cut-ting. In [29], the transient behavior of cables unwinding from inner-winding cylindrical spool dispensers was investigated.

Given results were an inspiration for us to deal with CWU systems and from this interest novel papers were made.

The aim of paper [30] is the analysis and definition of the phenomenon of nonlinear and pulsed nature of the dynamic process of the rope winding (unwindung) on the winch.

This process is characterized with sudden and abrupt jumps of dynamic variables which describe the rope winding (unwinding) process. Because of that, we have named this process: process of the rope „jumpy“ nonlinear in one row radially multilayered winding (unwinding) on the winch. Because of the easier understanding of this „jumpy“ concept of the winding (unwinding) process, we have first analyzed this concept under idealized circumstances - when the rotational speed of the winch is constant.

As a solution of analyzed problem, novel winch was developed which was patented as Registration number 57921 B1 [31]. . New constructive solutions of winches for single-row radial multi-layered cable smooth winding/unwinding on a winch are described in [32]. Two new structural solutions of winches have been defined. The nonlinear phenomenon of cable smooth winding/unwinding process on the winch by using one of the two proposed constructive solutions has been defined and analyzed. To facilitate understanding of this concept, the cable winding/unwinding process on only one winch has been analyzed. The obtained variables which characterize the kinematics of the cable smooth winding/unwinding process are nonlinear and smooth. This result is important because the systems for smooth cable winding/unwinding process on the winch could be parts of any cables driven mechanism. These systems can be used in various fields of human activity.

Based on analysis and synthesis of different types of CWU systems, in paper [33] a general form of mathematical model of these systems is presented. Mathematical model of CWU system indicates the impact of all the dynamic parameters of this system on its dynamic response. Theoretical contribution will be confirmed through experimental analysis of one chosen type of CWU system.

In Section 2, a detailed description of some types of CPR systems developed and general form of mathematical model is given. Most of this section is devoted to the CPR kinematic model, which is directly involved in the development of its dynamic model. See Subsection 2.1. Several cases of the systems are analyzed for same conditions in the Subsections 2.2 and 2.3.

In this Section 3, several types of CWU systems are analyzed and modeled. In Subsections 3.1-3.3, different types of CWU systems are presented. The general form of mathematical model of CWU system is formulated in Subsection 3.4. By using the new mathematical model, the program package CWUSOFT is presented in Subsection 3.5. This program package is used to perform simulation of the motion of one chosen CWU system's load in Subsection 3.6. In Section 3.7, experimental confirmation of theoretical contributions is presented.

The conclusions and observations are presented in the last part of the paper, Section 4.

2. CPR systems

The shape of the work space (plane, spatial), number of motors, number of hanging points, and total number of ropes, characterize the structure of the system. Individual analysis of each of new elements does not make sense, because it is important that the combined affect is analyzed and defined.

The shape of the work space depends in the dimensions and shape of the space where the camera needs to move. Basis of spatial systems may have different geometric shape (above view): triangle, quadrilateral, pentagon, and hexagon; except that they have a third dimension, i.e. height. Plane CPR systems are not the subject of this work. Spatial CPR systems whose working space is in the form of parallelepiped are of particular importance. They have the task of camera spatial movement and they are the topic of this work.

Number of hanging points is usually dictated by the need to achieve certain camera functions in certain dimensions of space.

Number of engines depends on the design of the mechanism and DOFs of the CPR mechanism.

This paper will be limited to the types of structures that were developed in Mihajlo Pupin Institute. We will complete further exposure related to the limited type of construction as defined in Figs. 7-12.

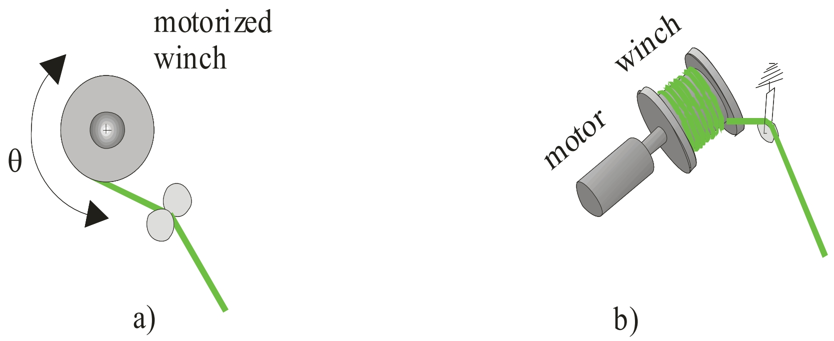

FIGURE 1. The motor that winds and unwinds the rope at the same side.

Mode of the motor operation is important element for functioning CPR system.

In the Figs. 1-3 represents the type of motor. Each example has two pictures related to view:

a) in direction of shaft axe motor,

b) in space.

The motor which, from the same side, winds or unwinds the rope is used for the RSCPR system described in Fig. 7 and in RFCPR system described in Fig. 8.

Motor presented in Fig. 2. is used for systems CPR-A, CPR-B, CPR-C and CPR D presented in Figs. 9-12, respectively.

The motor presented in Fig. 3 winds the ropes at one side. The motor is used to wind up the two ropes about the coil only in same direction. This motion produces winding or unwinding of both ropes at the same time. Motor presented in Fig. 3. is used for systems CPR-A, CPR-B, CPR-C and CPR D presented in Figs. 9-12 respectively.

Different suspension systems with cameras are presented in following figures.

In the Figs. 4-6 represents the type of the hanging. Each example has two pictures related to view:

a) 3D space view,

b) top view.

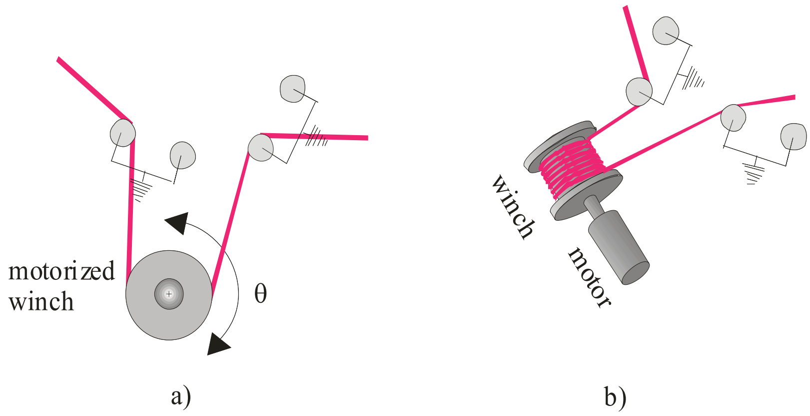

FIGURE 2. The motor that winds the rope at one side, and unwinds it at the other side.

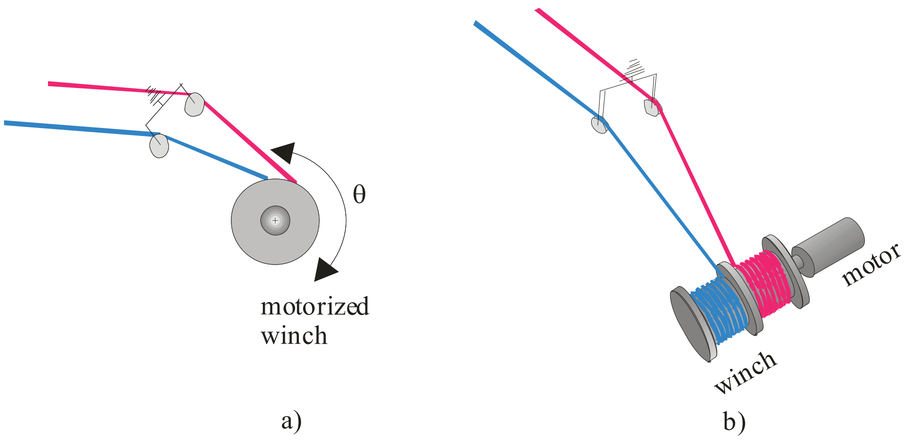

FIGURE 3. The motor that winds and/or unwinds two ropes at the same time from the same side.

The 3D recorded space has a parallelepiped shape with length d, width s, and height v in which the camera is connected with the parallel ropes. See Fig. 7-12. The connecting points at the camera carrier are used to safely support the camera. The distances between these points and the center A of camera are $\delta_{x1}, \delta_{x2}, \delta_{y1}, \delta_{y2}$. See Figs. 4-6 and compare with Figs. 7-12. These dimensions are very small in comparison with the complete 3D recorded space. From this observation it is clear that $\delta_{x1}\approx 0, \delta_{x2}\approx 0, \delta_{y1}\approx 0, \delta_{y2}\approx 0$. It is also assumed that the height of pivot point A is z which is equal to the heights of all four connecting points.

This fact allows us to choose a point A as a hanging position of the camera carrier for all ropes, see Figs. 7-12. This assumption simplifies the definition of geometric relations between camera carrier motion in Cartesian coordinates and coordinated motions of all motors.

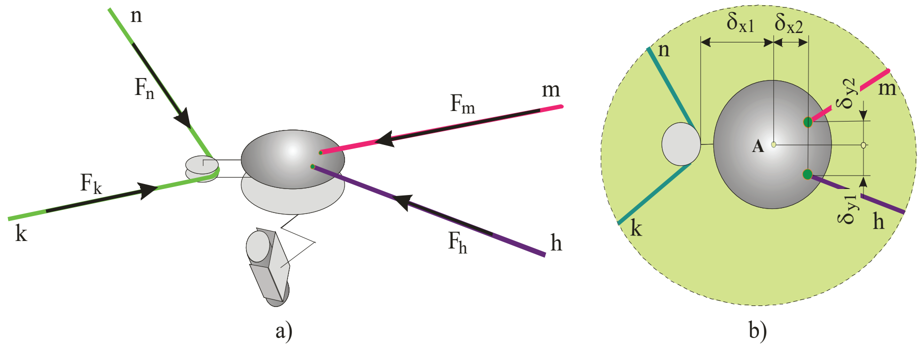

FIGURE 4. The connecting points at the camera carrier for RSCPR system, a) 3D space view, b) top view.

2.1. The Mathematical Model of Different Type CPR Systems. From this observation (see Figs. 7-12) it is clear that each direction *k, h, m, n* can have one or two parallel ropes.

The graphical representation different types of the CPR systems are shown in Figs. 7-12. The camera carrier of the CPR structures is guided through the work area of the parallelepiped shape with ropes connected with three winches, each of them powered by the motor.

The ropes of the pulley system are run on the winches (reel) 1, 2, 3, powered by the motors. The ropes coil or uncoil on the winches of radius R_1, R_2, and R_3. The motors rotate winches directly and its angular positions are θ_1, θ_2, and θ_3. This motion moves the camera in the *x, y, z* Cartesian coordinates.

The first step towards the dynamic model of the CPR is the development of its kinematic model. This calculation involves accurate definition of the geometric relationship between the camera motion in the *x, y, z* Cartesian space (external coordinates) and motor angular positions θ_1, θ_2, θ_3, (internal coordinates).

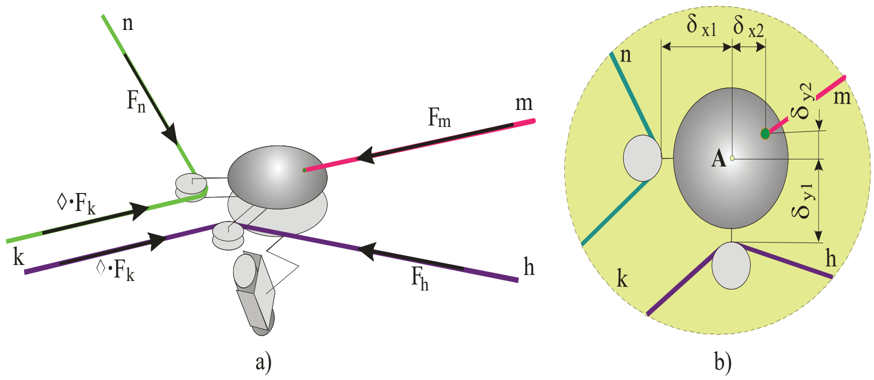

FIGURE 5. The connecting points at the camera carrier for RFCPR system, a) 3D space view, b) top view.

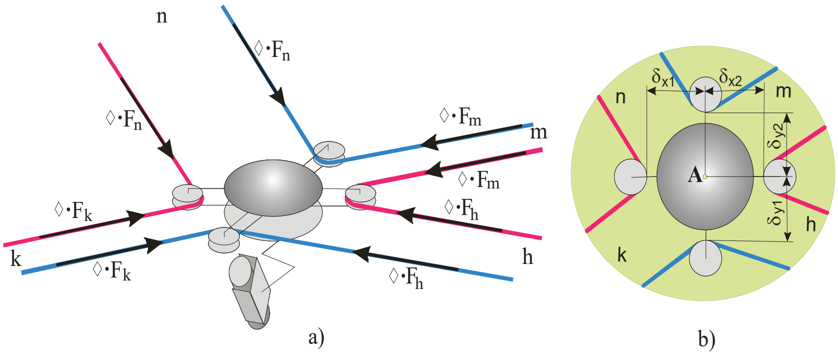

FIGURE 6. The connecting points at the camera carrier for CPR-A, CPR-B, CPR-C, and CPR-D systems, a) 3D space view, b) top view.

The relation between the internal and external coordinates is defined by the Jacobian matrix *J*, which relates the velocities of the external coordinates $\dot{p} = [\dot{x} \quad \dot{y} \quad \dot{z}]^T$ with the velocities of the internal coordinates $\dot{\phi} = [\dot{\theta}_1 \quad \dot{\theta}_2 \quad \dot{\theta}_3]^T$, presented in equation (1) and (2).

$$\dot{\phi} = J \cdot \dot{p} \tag{1}$$

$$J = \begin{bmatrix} J_{11} & J_{12} & J_{13} \\ J_{21} & J_{22} & J_{23} \\ J_{31} & J_{32} & J_{33} \end{bmatrix} \tag{2}$$

For the generation of any trajectory in *x, y, z* space, it is necessary to provide very precise and mutually coordinated motion of all three motors $\theta_1, \theta_2, \theta_3$.

This procedure is named KinCPR-Solver (Kinematic Cable Parallel Robot Solver). This is a novel methodology for the CPR system kinematic modeling. This methodology KinCPR-solver represents a general guideline for solving any kinematic structure of the CPR system types.

The Jacobian matrix *J* in equation (1) is full matrix. The elements of this matrix beyond diagonal show the strong coupling between the external and internal coordinates.

The camera carrier together with the camera represents a small system in a comparison to the complete work area. In that case the small system has neglectable moments of inertia about each axis of the local coordinate system at the point *A*.

In the camera dynamics modeling, the camera is represented as a material particle with three degrees of freedom in the *x, y, z* Cartesian coordinates system.

The kinetic energy E_k and potential energy E_p of the camera carrier motion with mass *m* are given in the following equations:

$$E_k = \frac{1}{2} \cdot m \cdot \dot{x}^2 + \frac{1}{2} \cdot m \cdot \dot{y}^2 + \frac{1}{2} \cdot m \cdot \dot{z}^2 \tag{3}$$

$$E_p = m \cdot g \cdot z \tag{4}$$

In this analysis the ropes are assumed to be rigid. In that case the mathematical model of the described system has the following form:

$$u = G_v \cdot \ddot{\phi} + L_v \cdot \dot{\phi} + S_v \cdot M \tag{5}$$

The vector equation (5) is developed by applying the Lagrange's equation on generalized coordinates θ_1, θ_2, θ_3.

Where: $u=[u_1\ u_2\ u_3]^T$, $G_{v(3x3)}=diagG_{vi}$, $L_{v(3x3)}=diagL_{vi}$, $S_{v(3x3)}=diagS_{vi}$.

The resultant load moment M is defined with the vector's equation (6).

$$M = \begin{bmatrix} F_1 \cdot R_1 \\ F_2 \cdot R_2 \\ F_3 \cdot R_3 \end{bmatrix} \tag{6}$$

The Lagrange principle of virtual work has been used to find the relation between the resultant moment M and external force F.

$$(M)^T \cdot \dot{\phi} = F^T \cdot \dot{p} \tag{7}$$

The external force F is given in the following equation:

$$F = F_p + P_p \tag{8}$$

$$F_p = m \cdot (\ddot{p} + a_c\ ) \tag{9}$$

The external force F represents the sum of the inertial force F_p which is acting on the camera carrier described in equation (8), and the perturbation force P_p which is disturbing the camera motion.

Vector $a_{cc}=[0\ 0\ -g]^T$ represents the gravitational acceleration.

By substituting the equation (1) into the equation (7) the following equation is generated:

$$(M)^T \cdot J \cdot \dot{p} = F^T \cdot \dot{p} \tag{10}$$

By dividing the equation (10) with $\dot{p}$, the equation (11) is obtained.

$$(M)^T \cdot J = F^T \tag{11}$$

By transposing the equation (11), the equation (12) is obtained.

$$(J)^T \cdot M = F \tag{12}$$

From the equation (12), the equation (13) is expressed:

$$M = \left((J)^T\right)^{-1} \cdot F \tag{13}$$

$$O = \left((J)^T\right)^{-1} \tag{14}$$

The equation (13) cannot be directly applied to the system presented in the Fig. 8, because the system has two ropes in k direction. This situation causes the Jacobian matrix J to be corrected using the factor ◊.

◊ is a factor which multiplies only the direction where there are two parallel ropes. In the *k* direction, a force in each rope is multiplied by ◊, which is a half of the whole force F_k. See Fig. 8b).

Observed RFCPR system has two ropes from a camera carrier to the wall anchors (line *k*), and one rope from the camera carrier to the remaining three-point suspension (line *h, m, n*). The elements of the matrix *J* which contain the length k are multiplied by a factor ◊.

Some elements of the Jacobian matrix *J* have the following values $J_{11} = \frac{x}{R_1 \cdot k} + \frac{x}{R_1 \cdot n}$, $J_{12} = \frac{y}{R_1 \cdot k} - \frac{(s-y)}{R_1 \cdot n}$, and $J_{13} = \frac{z}{R_1 \cdot k} + \frac{z}{R_1 \cdot n}$ while elements of the adopted Jacobian matrix $J_\Diamond$ have values $J_{\Diamond 11} = \Diamond \cdot \frac{x}{R_1 \cdot k} + \frac{x}{R_1 \cdot n}$, $J_{\Diamond 12} = \Diamond \cdot \frac{y}{R_1 \cdot k} - \frac{(s-y)}{R_1 \cdot n}$, and $J_{\Diamond 13} = \Diamond \cdot \frac{z}{R_1 \cdot k} + \frac{z}{R_1 \cdot n}$, respectively.

This situation causes the Jacobian matrix *J* to be corrected using the factor ◊.

$$J_\Diamond = f(\Diamond, J) \tag{15}$$

The adapted Lagrange principle of virtual work defined in equation (16) has been used for solving the complex relation between the resultant moment (acting as a load at the first, second and third motor shaft) and external force (acting at the camera carrier) for RFCOR system.

$$M = \left(\left(J_\Diamond\right)^T\right)^{-1} \cdot F \tag{16}$$

The equation (13) cannot be directly applied to the system from the Fig. 9-12, also, because of the following reasons:

The system has two ropes in each direction. The equation (13) has been corrected using the factor *◊=0.5*. This correction affects the forces F_k, F_h, F_m, and F_n, which are multiplied by the factor ◊, and their values are $\Diamond \cdot F_k$, $\Diamond \cdot F_h$, $\Diamond \cdot F_m$, and $\Diamond \cdot F_n$.

The Jacobian matrix *J* has been changed accordingly.

$$J_\Diamond = \Diamond \cdot J \tag{17}$$

This is the first reason why the Lagrange's principle of virtual work has been adapted. See equation (17).

The force F_3 multiplied by the radius R_3 produces a moment load at the motor *3*. The two forces at the motor *3* have the same direction and the intensity, which is $\Diamond \cdot F_3$. See Figs. 9-12. The force F_3 has two equal components of the $\Diamond \cdot F_3$ value. The total force F_3 is the sum of these two components: $F_3 = 2 \cdot \Diamond \cdot F_3$.

The motor *3* simultaneously unwind or wind both ropes.

The motor *3* is used to synchronize winding or unwinding these two ropes.

The adopted matrix $J_\Diamond$ (defined in equation (17)) components $J_{\Diamond 31}$, $J_{\Diamond 32}$, $J_{\Diamond 33}$ **s**hould be multiplied by two, which will produce the double-adapted Jacobian matrix $J_{x\Diamond}$.

These facts significantly influence the Jacobian matrix, which has a new form expressed in equation (18):

$$J_{x\Diamond} = \begin{bmatrix} \Diamond \cdot J_{11} & \Diamond \cdot J_{12} & \Diamond \cdot J_{13} \\ \Diamond \cdot J_{21} & \Diamond \cdot J_{22} & \Diamond \cdot J_{23} \\ 2 \cdot \Diamond \cdot J_{31} & 2 \cdot \Diamond \cdot J_{32} & 2 \cdot \Diamond \cdot J_{33} \end{bmatrix} \quad (18)$$

This change represents the second adaptation of the Jacobian matrix.

Using the equation (18) the moment mapping matrix O is generated below:

$$O = \left(\left[J_{x\Diamond} \right]^T \right)^{-1} \quad (19)$$

The connection between the resultant moment M and external force F is established. See equation (20).

$$M = O \cdot F \quad (20)$$

By substituting equations (20) into the equation (5), the dynamic model of the CPR has been generated:

$$u = G_v \cdot \ddot{\phi} + L_v \cdot \dot{\phi} + S_v \cdot O \cdot F \quad (21)$$

The moment mapping matrix O represents a strong coupling between the presented motors.

This would be a general form of mathematical model of different CPR system type: RSCR, RFCPR, CPR-A, CPR-B, CPR-C and CPR-D. It was clearly emphasized that different configurations of these systems result in different Jacobian matrix J and moment mapping matrix O of every system. For the same reason, the Lagrange's principle of virtual work in original form is not applicable for the systems: RFCPR, CPR-A, CPR-B, CPR-C and CPR-D, but it needs to be modified.

Through the comparative results, it will be shown how motor selection can significantly affect the motion dynamics of a camera carrier. This emphasizes the importance of selecting the type of motor as a very important component of the CPR system.

Control law is selected by the local feedback loop for position and velocity of the motor shaft in the following equation:

$$u_i = K_{lpi} \cdot (\theta_i^o - \theta_i) + K_{lvi} \cdot (\dot{\theta}_i^o - \dot{\theta}_i) \quad (22)$$

2.2. Program Packages. In this paper, we have developed the 6 types of CPR systems: RSCPR, RFCPR, CPR-A, CPR-B, CPR-C, and CPR-D system. They are shown in Figs. 7 -12, and they are briefly described via their program packages.

RSCPR System. The program system ORIGI is generated in MATLAB. This program system presents the analysis, synthesis and modeling of the selected Rigid ropes S-type Cable-suspended Parallel Robot (RSCPR).

The important characteristic of this system is its geometric construction which defines the kinematic model through the Jacobian matrix J_S.

The relationship between external and internal forces is defined by the Lagrange principle of virtual work. The Jacobian matrix is directly involved in the application of the Lagrange principle of virtual work and generation of the dynamic model of the RSCPR system. The software packages named ORIGI has been used for the RSCPR model verification.

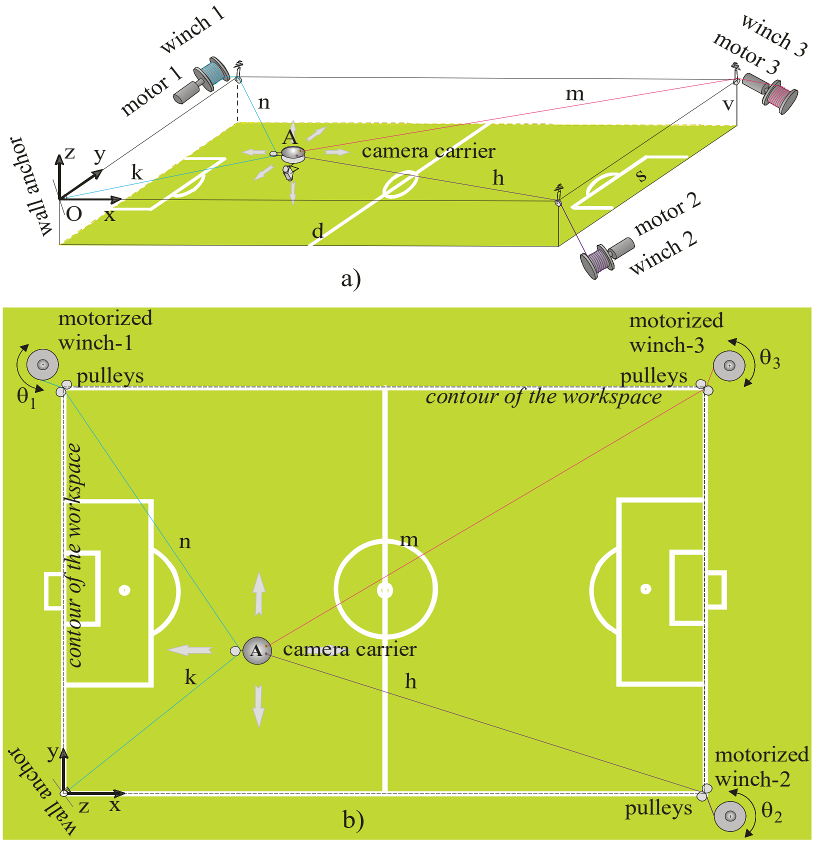

FIGURE 7. RSCPR system, a) in the 3D space, b) top view.

RFCPR System. The program system ORVER is generated in MATLAB. This program system presents a methodology for kinematic and dynamic modeling of the selected Rigid ropes F-type Cable-suspended Parallel Robot (RFCPR) with the un - stretchable ropes.

The RFCPR system is used for the workspace observation. The complex construction of the selected aerial robot requires in depth study of the relationship between external and internal forces. The Jacobian matrix J_F plays an important role in developing the RFCPR dynamic model.

This system is constructed such that its geometric structure requires the adaptation of the Lagrange principle of virtual work. The RFCPR model is utilized for very complex tasks using the intelligent control system. The software packages named ORVER has been used for the RFCPR model verification.

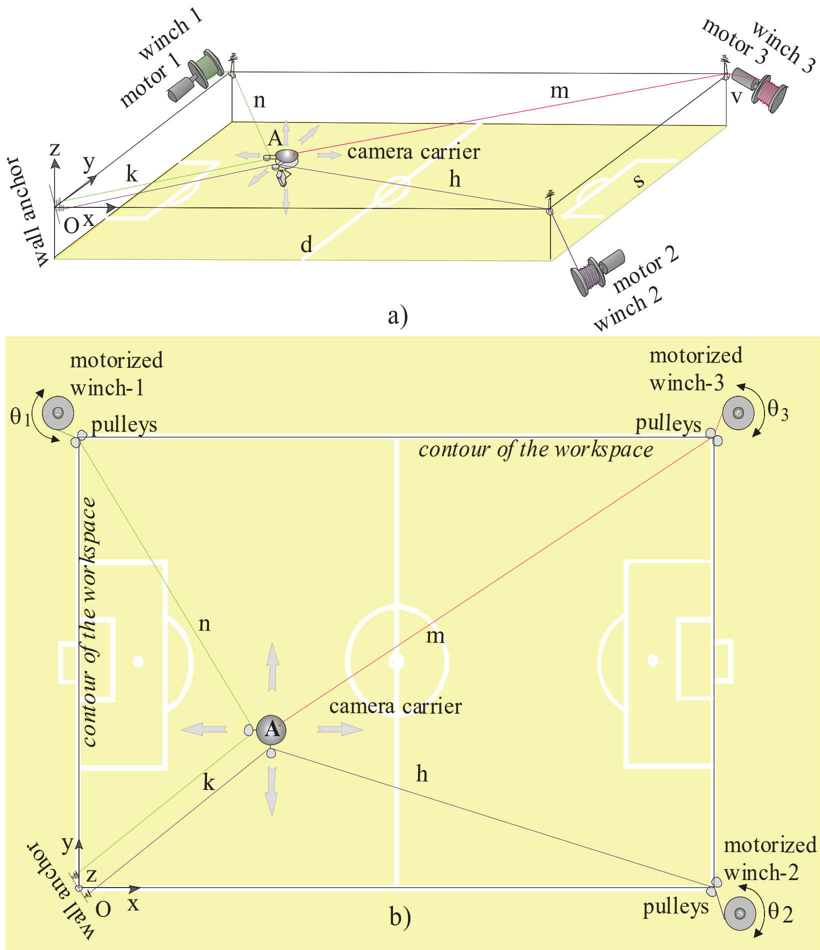

FIGURE 8. RFCPR system, a) in the 3D space, b) top view.

CPR-A System. The software package AIRCAMA is also synthesized for the same purpose, and it offers a choice of parameters of the system and analysis of its dynamic behavior as well as with the purpose of presenting comparative results.

Defined algorithm is applied to any size workspace selection, with the camera weight, the desired speed cameras and so on, of CPR-A system from Fig. 9. Depending on the choice of these parameters' types and characteristics of each motor are chosen.

Activating the program package, it is possible to make the analysis of the results, where it can be concluded if the selection of motor types is correct, or whether it meets the requirements. It is also possible to analyze the coordination of motion in relation to the desired requests. It is possible to observe any motion from the selected workspace. The formulated program package AIRCAMA (based on its mathematical model) has a special significance because it is the foundation for further development and implementation of this system.

Program package AIRCAMA that is synthesized specially for the purpose of comfort analysis of such complex system served for obtaining simulation results.

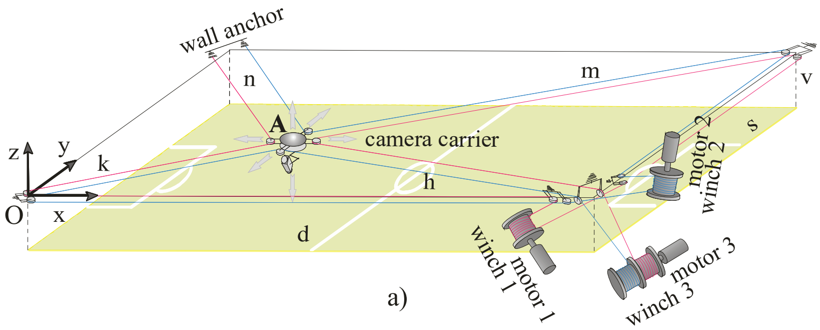

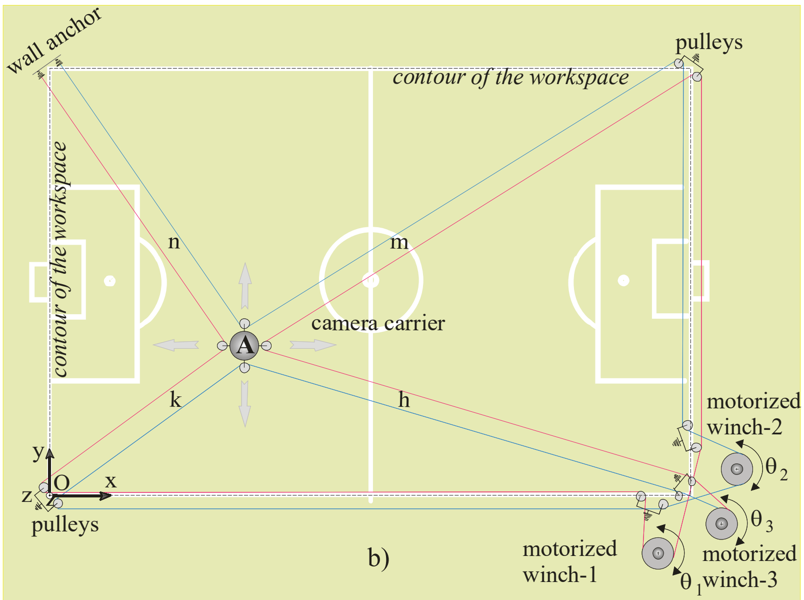

FIGURE 9. CPR-A system, a) in the 3D space, b) top view.

CPR-B System. The aim of this program package AIRCAMB is a detailed synthesis and analysis Cable-suspended Parallel Robot, CPR-B system from Fig. 10, which should enable their strong progress. This would be reflected in the implementation of highly-automated system that would lead the camera precisely in space with minimum participation of human labor. Setting and achieving this goal provides a much wider possibilities for its future use.

The unique general type of the CPR-B mathematical model is defined. Kinematic model is generated for the system via Jacobian matrix. An adequate choice of generalized coordinates (the internal coordinates), provides a mathematical model that illuminates the mapping of internal (resultant forces acting on the shaft of each motor) and external forces (acting on a camera carrier) by the Jacobian matrix on motion dynamics of each motor. Such an operation of this system can provide only with application of his high-fidelity mathematical model during the synthesis and analysis, which would further enable the development and application of modern control law.

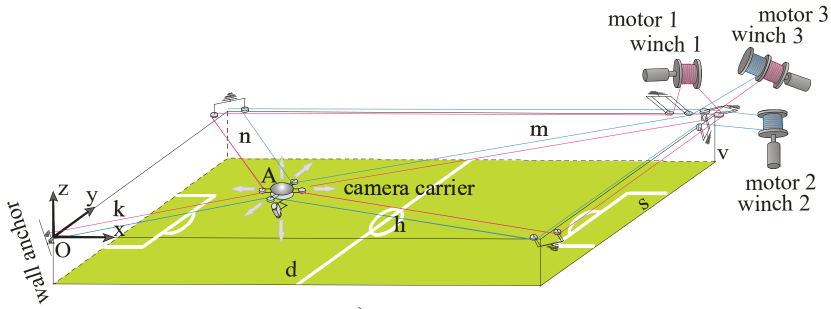

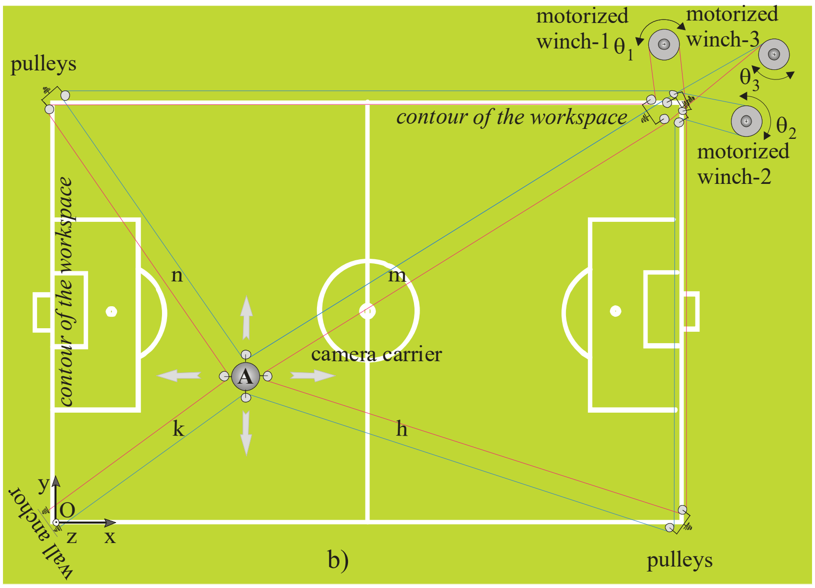

FIGURE 10. CPR-B system, a) in the 3D space, b) top view.

The modeling task is solved as software so that a user should choose the system parameters that provide the possibility of the analysis of its dynamic behavior.

There is a possibility of extension of program system AIRCAMB from different aspects according to the users' needs. This program system is generated in MATLAB.

CPR-C System. In this program system a special case of the constructive Cable Suspended Parallel Robot - CPR model solution, has been analyzed. This model is named CPR-C, and it is presented in Fig. 11.

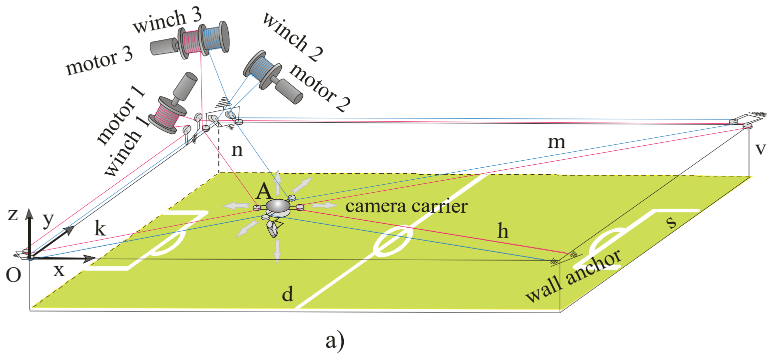

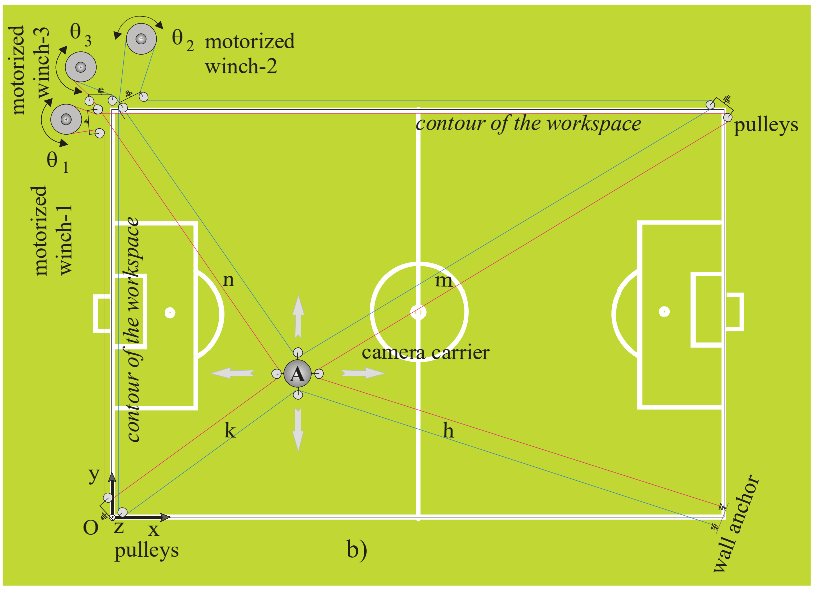

FIGURE 11. CPR-C system, a) in the 3D space, b) top view.

The purpose of this research is to implement the program system AIRCAMC and possibly improve the model for the future modernization, autonomy and intelligent behavior of the aerial robot named CPR-C. The form of highly complex mathematical model is necessary in order to achieve the desired motion of the camera carrier in the parallelepiped workspace shape.

CPR-D System. This system is defined by specific features such as ropes which are led double in four directions, as well as the motor which on one side winds the rope and unwinds it on the other side. Each of these properties must be included within the CPR-D mathematical model which will influence the change of the Lagrange principle of the virtual work.

The CPR-D system is modeled and analyzed by the software package AIRCAMD, which is used for validation of applied theoretical contributions.

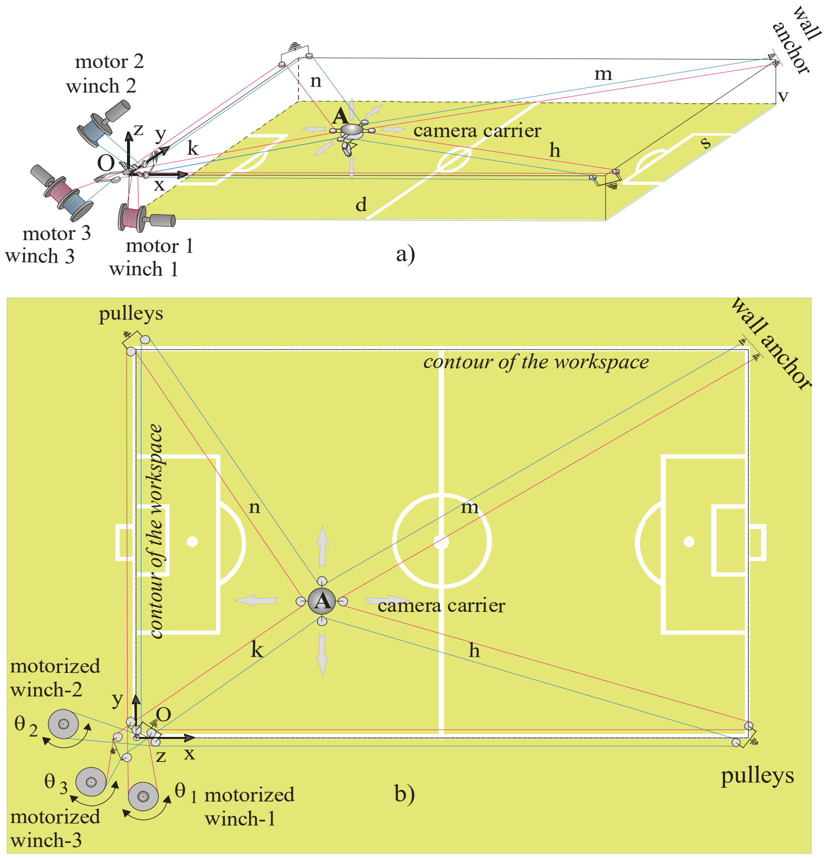

FIGURE 12. CPR-D system, a) in the 3D space, b) top view.

The modeling task is solved as software AIRCAMD so that a user should choose the system parameters that provide the possibility of the analysis of its dynamic behavior. This program system is generated in MATLAB.

The software package includes three essential modules, which are the kinematic, dynamic and motion control law solvers for the considered CPR system. The most important element of the CPR system is the motor mathematical model which is an integral part of software package. Through the simulation results it is shown that the dynamic characteristics of the motor significantly affect the response of the system and its stability. The camera carrier motion dynamics directly depends of the mechanism dynamic parameters.

2.3. Simulation Results. We will show the comparative analysis of, only, these systems: CPR-A, CPR-B, CPR-C, and CPR-D, because they look same when one first looks at them. Mathematical models of these configurations show their difference, which is confirmed by the simulation results.

In order to make the results comparable, the CPR-A, CPR-B, CPR-C, and CPR-D models have been analyzed using the same desired trajectory and the same all other system parameters. The camera moves in the 3D space in x, y, and z directions.

The camera carrier has starting point $p_{start}^{o}=[1.6\ 1.3\ -0.5](m)$, and the end point $p_{end}^{o}=[1.0\ 0.7\ -0.2](m)$.

A camera carrier is under the influence of the disturbance force $P_p=[0\ 110\cdot\sin(4\pi\cdot t)\ 0]^T$, which simulates the impact of wind attack.

The camera moves in x, y, and z directions and its velocity has a trapezoidal form with maximum velocity $\dot{p}^{o}_{\max}=0.417(m/s)$, as shown in Fig. 13c).

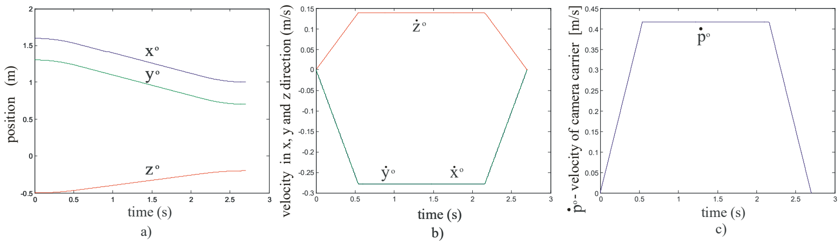

FIGURE 13. The reference trajectory motion of a) position x^o, y^o, z^o, b) velocity $\dot{x}^o$, $\dot{y}^o$, $\dot{z}^o$, c) velocity of the $\dot{p}^o$ of camera carrier (CPR-A, CPR-B, CPR-C, and CPR-D systems).

The selected motors are by Heinzman SL100F and selected gear boxes are HFUC14-50-2A-GR+belt.

The system responses, for all four Examples are shown in Figs. 13-16.

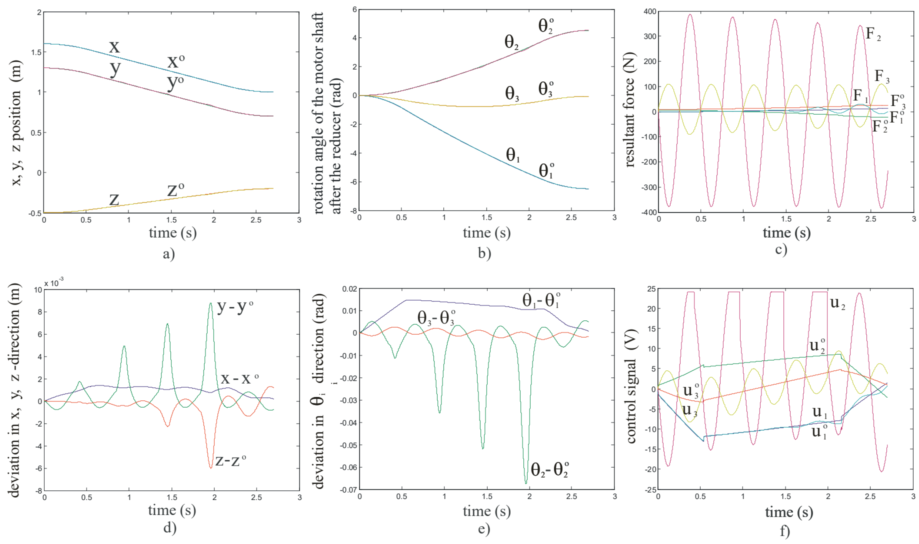

FIGURE 14. Simulation results for CPR-A system.

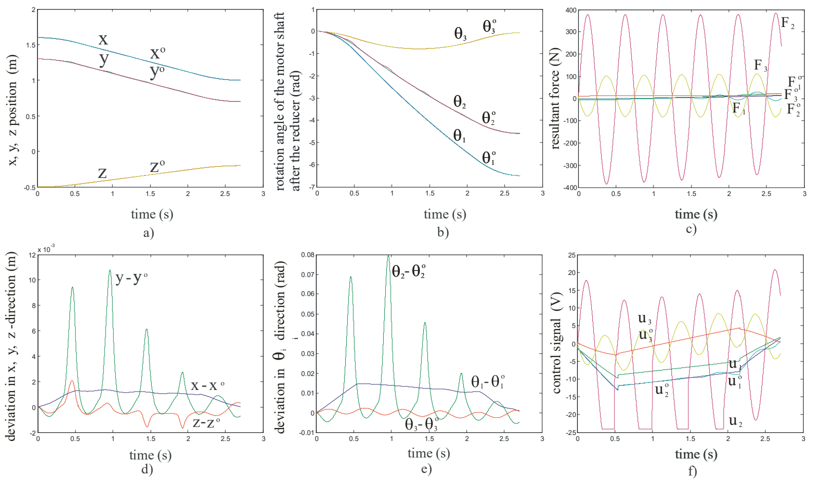

FIGURE 15. Simulation results for CPR-B system.

In the Fig. 13-16. represents the results for selected case studies (Examples 1-4). Each example has six pictures related to:

a) the camera carrier position at the reference and the real frames,
b) the motor shaft position at the reference and the real frames,
c) the forces in the ropes at the reference and the real frames,
d) the deviation between the real and the reference trajectory of the camera carrier,
e) the deviation between the real and the reference trajectory of the motor shaft positions,
f) the reference and the real control signals.

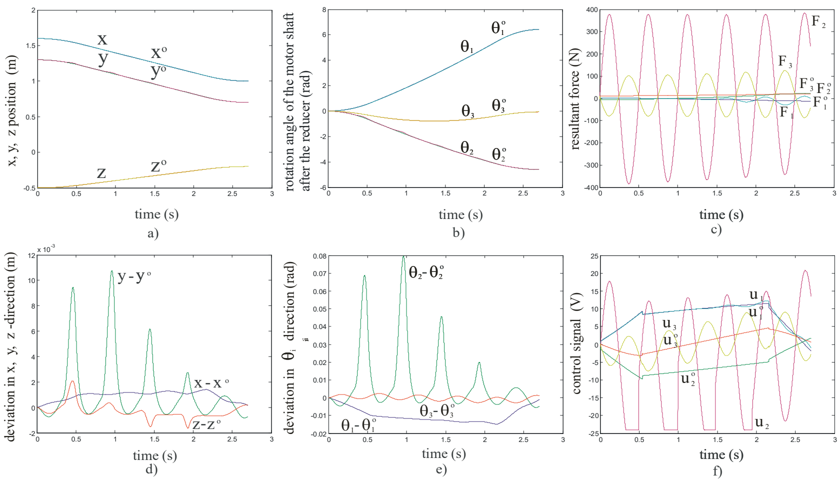

FIGURE 16. Simulation results for CPR-C system.

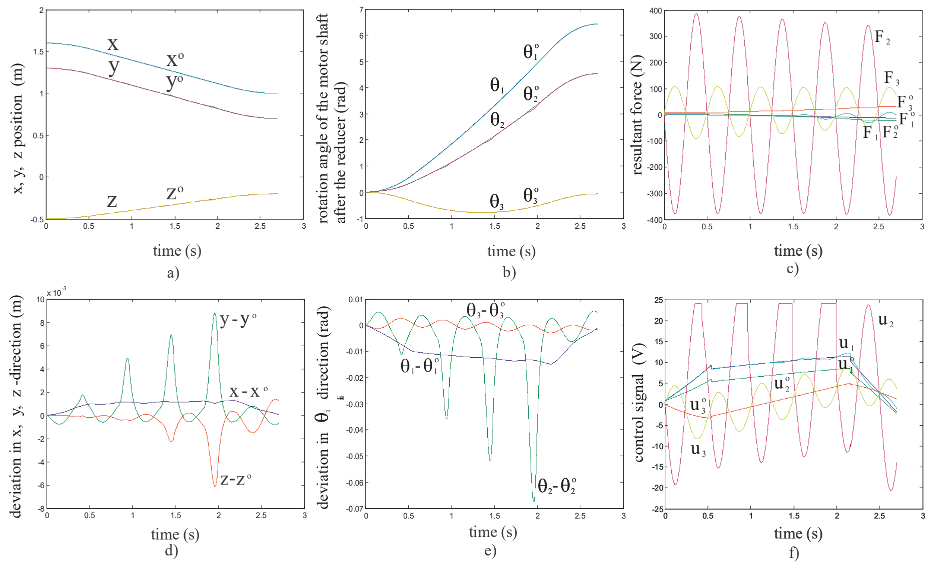

FIGURE 17. Simulation results for CPR-D system.

In this Section, six types of CPR systems: RSCPR, RFCPR, CPR-A, CPR-B, CPR-C, and CPR-D system, are presented, modeled and analyzed. These are systems with 3 DOF. In next Section, one of subsystems of CPR system which describes nature of the dynamic process of the rope winding (un-winding) on the winch will be described. This subsystem contais following elements: motor, gear, winch, pulley and cable that is wound/unwound on the winch. This subsystem is called cable winding/unwinding system, or: CWU system.

3. Different Types of Cable Winding/Unwinding Systems

In this part of paper, several types of CWU systems will be presented. Their constructive differences will be indicated. The CWU system consists of: motor, gear, winch, pulley and cable that are wound/unwound on the winch.

3.1. Standard System for Single-row Radial Multi-layered CWU Process. This construction of CWU system has a circular shape of the winch and it is shown in Fig. 18.

Detailed description of this system is presented in [30]. It was shown that this solution of the winch has adverse effects on the system's dynamic response and it causes instability and oscillations of the system. This structural instability of the winch from Fig. 1 has inspired the authors of this paper to design a new form of the winch for performing the smooth process of CWU. This novel solution of CWU system for smooth winding/unwinding in two variants will be presented in the next sub-section. The new constructive solution of the system intended for performing smooth CWU process is presented in Fig. 19.

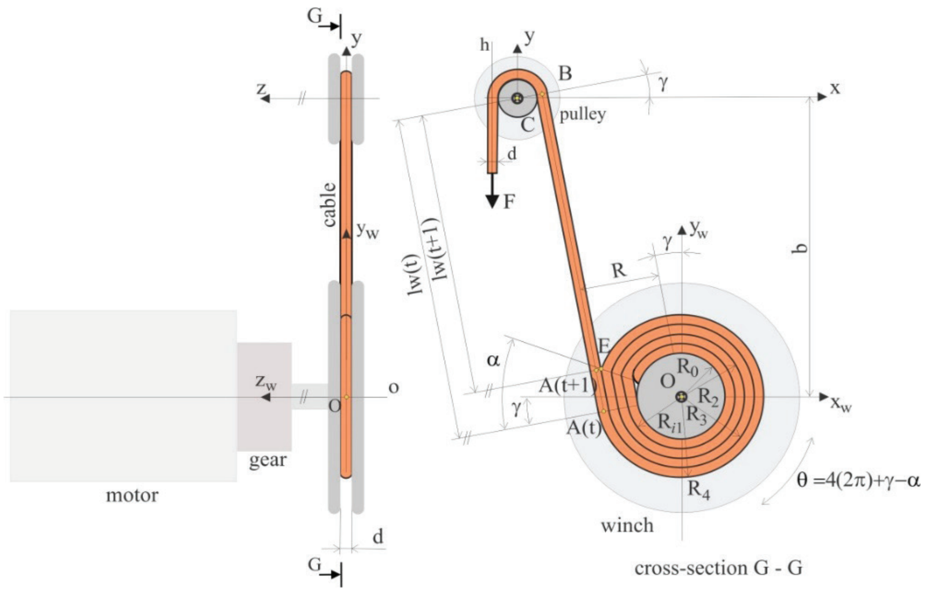

FIGURE 18. Standard system for single – row radial multi-layered CWU process.

3.2. Novel System for Smooth Single – row Radial Multi-layered CWU Process.

Fig. 19 presents two new constructive solutions of the winch can be used to avoid the constructively generated unstable and oscillatory behavior of the system from Fig. 18.

By using either of the two new constructive solutions of systems from Fig. 19: the two – cylinder winch (Fig. 19b) or the spiral winch (Fig. 19c), a smooth process of CWU on the winch is achieved.

1. The first constructive solution consists of two semicylindrical bodies of different radii and it is presented in Fig. 19b. Because of the characteristics of this winch, it has been named the two – cylinder winch.
2. The second constructive solution has a spiral shape and this winch is shown in Fig. 19c. It has been named the spiral winch.

See references [31, 32]. For further discussion, only the constructive solution from Fig. 19b will be used.

Fig. 20 presents two currently selected positions during the process of the CWU on the winch. Angle θ is measured as deflection between the line OE and negative part of the x_w axis, in positive mathematical direction, around point O. The process presented in Fig. 20 is named as: single – row radial multi-layered smooth CWU process on the winch or abbreviated smooth process of CWU on the winch. Dynamic variables which characterize the process shown in Fig. 20 are the following: winding/unwinding radius R, length l_w=AB, and angle γ.

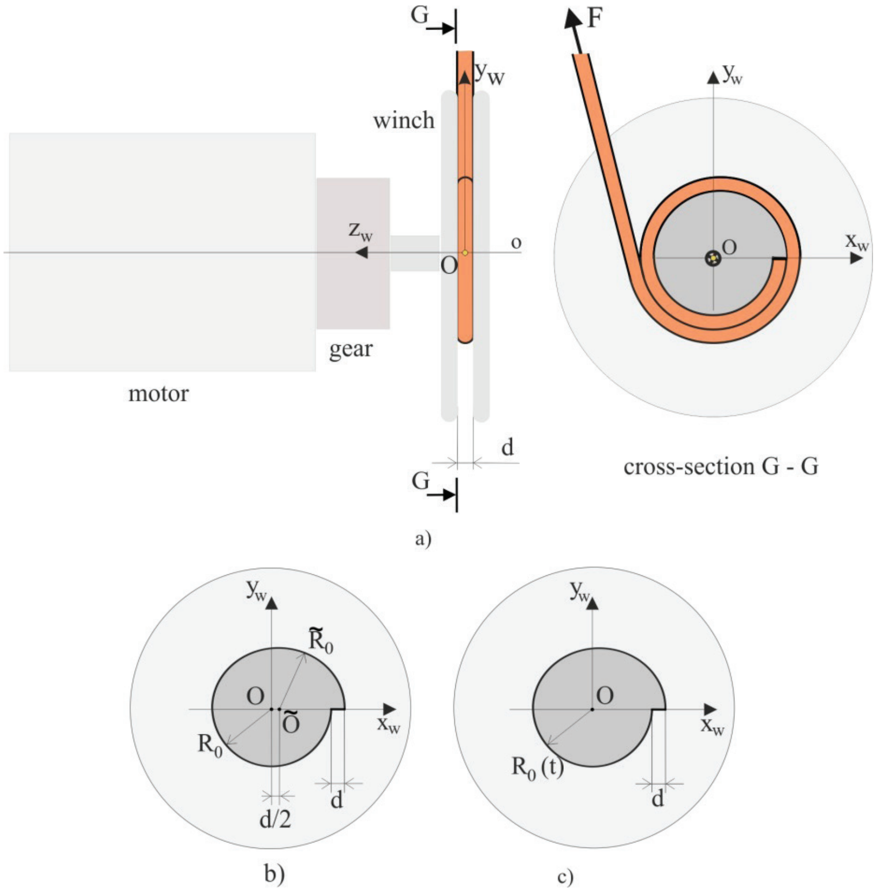

FIGURE 19. The new winch for performing a smooth CWU process: a) the winding/unwinding system, b) the two – cylinder winch, c) the spiral winch.

The change of these variables during the CWU process is smooth and nonlinear. Three phases of this process are to be observed:

a) in Fig. 20a the starting position of the CWU system is presented. In this case angle $\theta=0$.
b) in Fig. 20b the position of the smooth CWU process for the following values of angle θ is presented: $\gamma<\theta<\pi+\gamma$. In this period, dynamic variables R, $l_w=AB$, and γ of this process are constant, so this area has been named the *con* area,
c) in Fig. 20c the position of the smooth CWU process for the following values of angle θ is shown: $\pi+\gamma<\theta<2\cdot\pi+\gamma$. In this period dynamic variables R, $l_w=AB$ and γ of this process change their values, so this area has been named the *smvar* area. Changes of the characteristic variables are smooth and nonlinear, which is substantially different in comparison with the CWU process presented in Fig. 18.

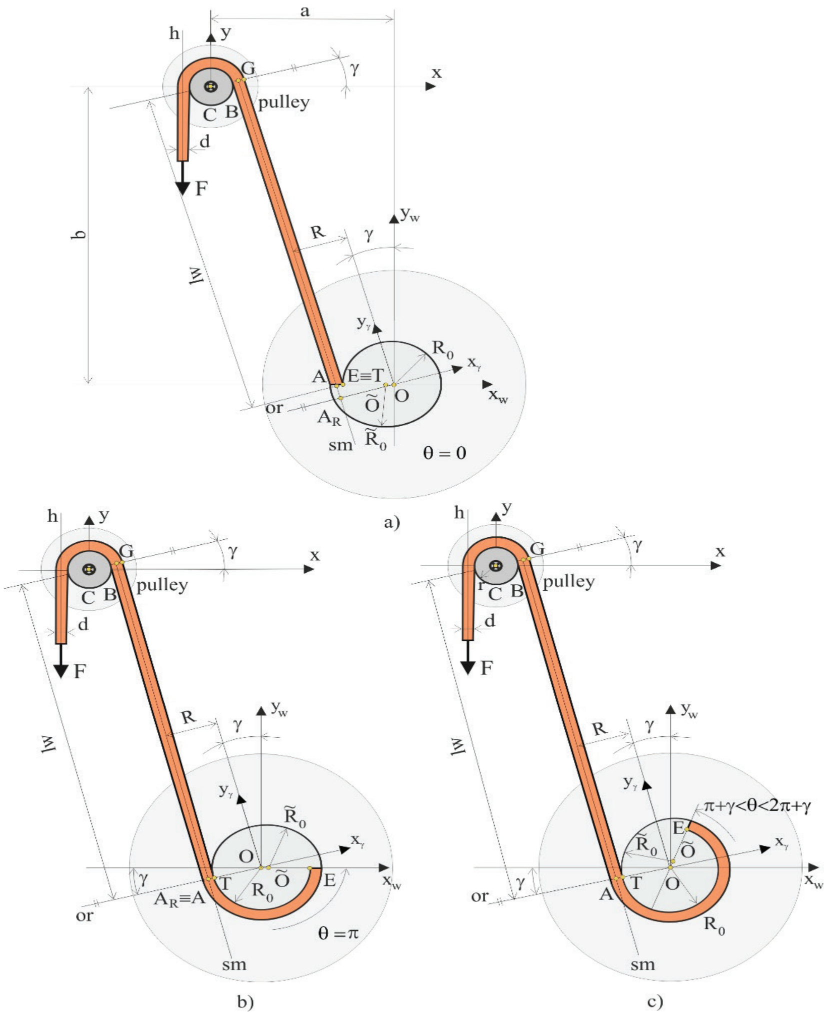

FIGURE 20. The positions of the smooth CWU system for: a) $\theta=0$ b) $\gamma<\theta<\pi+\gamma$, c) $\pi+\gamma<\theta<2\cdot\pi+\gamma$. .

During the process of the smooth CWU on the winch, areas *con* and *smvar* alternate cyclically. In the next sub-section, CWU system for multi-row radial and axial CWU process will be presented.

3.3. CWU System for Multi-row Radial and Axial CWU Process. This system is shown in Fig. 21. This type of CWU system is characterized with one motor and two gears. One gear rotates the winch, while the other gear moves it translatory based on its rotation. It can be seen that this system has one DOF. The motor which drives the winch has a rotary motion around the winch's axis. This motion is labeled as θ. For successful and controllable winding/unwinding of the cable on the winch, this winch must have a translatory motion along its z_w axis as well. This motion is labeled as c_θ. In [34], authors have defined the relation between motions c_θ and θ with Eqs. (13), (14) and Figs. 5, 6. It can be seen that these two motions have linear and ideal relation [34]. Many researchers, i.e. designers of CPR systems assume application of CWU systems which keep relation between these two motions linear. In case of any error in construction or disturbance during such system's application, idealized mathematical relation from [34] does not apply. In that case, relation between these two motions is defined with another mathematical formulation which will not be analyzed in this paper.

In order to facilitate understanding of this system's functionality, the first winding/unwinding layer will be described first. This example is shown in Fig. 22.

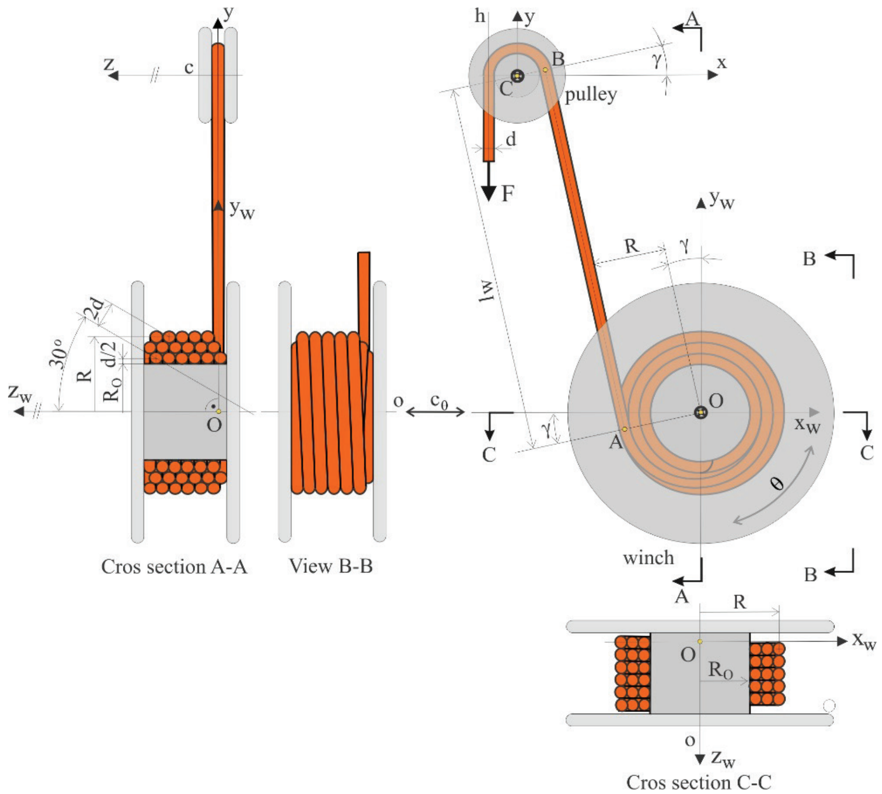

FIGURE 21. The system for multi-row radial and axial CWU process.

a) The first layer of winding.
Fig. 22 presents only the first layer of CWU process from Fig. 21. For example, authors of [20] only use cable winding/unwinding on the first layer, without the possibility and need for using the second layer, for implementation of their CWU system. The cable is only axially furled around the winch. Angular motion θ and translator motion c_θ must be coordinated for ideal cable furling

to be achieved. Unlike examples from Figs. 18-20, this phase of CWU implies constant characteristics *R, lw* and γ, so their first derivatives are zero. Radius of winding/unwinding is $R=R_0+d/2$. Next sub-section will present the CWU process of the second and third layer of system from Fig. 21.

b) The second and third layer of CWU process.
Fig. 23 shows the second layer of CWU process, while Fig. 21 presents the third layer of CWU process. Both figures relate to the same system, but because of easier understanding two different situations are examined. Like it was stated before, this type of the system implies coordinated angular θ and translator motion c_θ. Unlike the CWU phase on the first layer from Fig. 22, at the moment when the cable starts winding/unwinding on the second/third layer, characteristic variables R, l_w and γ become changeable, so their first derivatives are not zero.

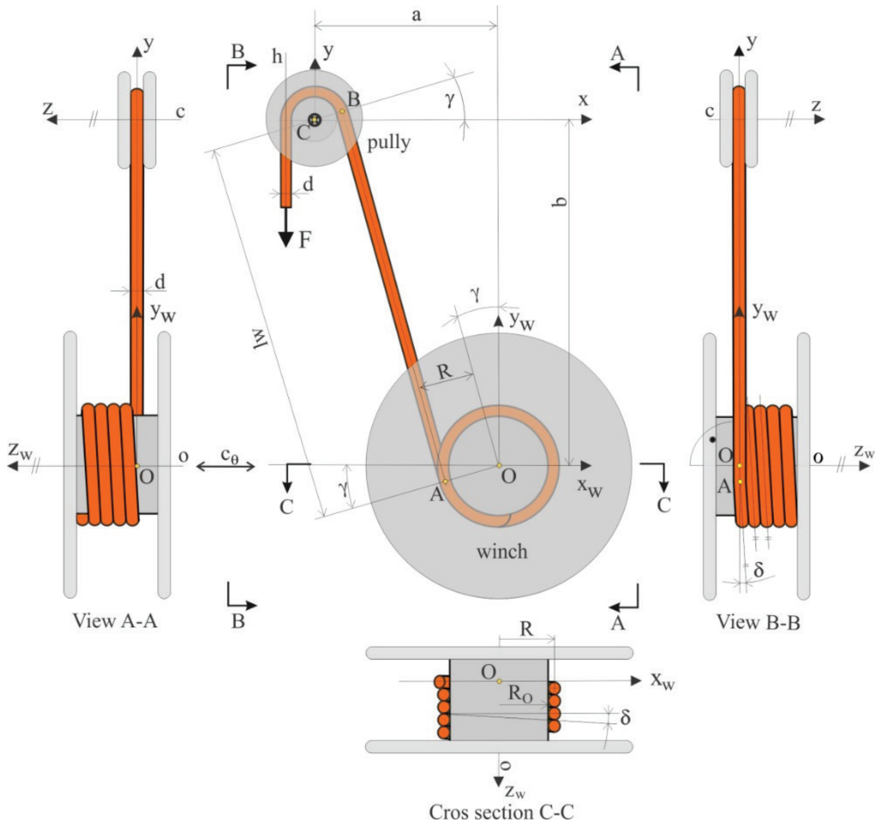

FIGURE 22. The system for multi-row radial and axial CWU process – one layer.

From Fig. 23 one can see that the winding/unwinding radius has a value of $R=R_0+d/2+2{\cdot}d/2$ in the C-C cross-section, while this value is $R=R_0+d/2+(2{\cdot}d/2){\cdot}cos(30^o)$ when system traverses the next 90^o, see the cross-section A-A. During the winding on the second layer, radius R continually increases and decreases each 90^o.

In the case of CWU process on the third layer from Fig. 22, one can see that radius R has a value of $R=R_0+d/2+4\cdot d/2$ in the cross-section C-C, while after system traverses next 90^o, the radius is $R=R_0+d/2+(4\cdot d/2)\cdot cos(30^o)$. This can be seen in the cross-section A-A from Fig. 21. During the winding on the third layer, radius R continually increases and decreases each 90^o. This change of radius R causes the change of length l_w and angle γ.

Following rule applies for CWU systems from Figs. 18-23: coordinate system x_w- y_w belongs to the plane defined by coordinate system x-y. This condition is constructively secured for systems from Figs. 18-20. For CWU systems shown in Figs. 21-23, this is secured with coordinated translational motion of the winch c_θ along z_w axis in dependence of angular rotation θ. This condition is especially noticeable in cross-section A-A shown in Figs. 21 and 22.

In the next Section, the general form of mathematical model of CWU systems from this Section will be presented.

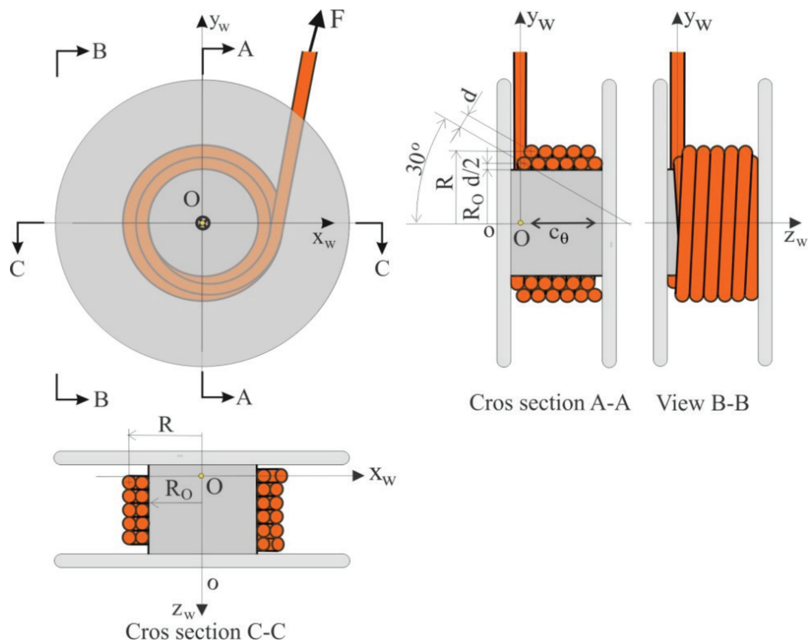

FIGURE 23. The system for multi-row radial and axial CWU process – two layers.

3.4. The General Form of Mathematical Model of CWU System. By observing the CWU systems from Figs. 18-23, it can be seen that they are different. Regardless of this fact, they are connected with same forms of kinematic and dynamic models. This will be presented in following sub-sections in detail. CWU system's cable is connected to a load via one pulley. Load's weight is labeled as m. Pulley's rotation axis is positioned at the coordinate system x-y. Whole system is presented in x-y plane. Coordinate system x_w- y_w is in the same plane as well.

The Kinematic Model of CWU System. It has been presumed that the position of the load, defined in the Cartesian coordinate system, is labeled as $p=[x\ y]^T$. These coordinates are named external coordinates. The winding/unwinding angle of the winch θ is defined around axis z_w which contains the point *O.* It is also presumed that winding/unwinding angle of the winch is defined as internal coordinate.

In the observed examples, motion direction of the load is in direction of the *y* axis. It is presumed that load's *x* coordinate has a constant value. The load's weight *m* is affected by gravitational acceleration and this defines the force *F.*

In general, it can be said that CWU systems from Figs. 18-23 are characterized with changeable dynamic variables: radius of winding/unwinding *R*, length of cable which connects pulley with winch l_w, and all the other dynamic variables.

In this Section, the changes of these variables will be included into CWU system's mathematical model. By introducing this novel phenomenon, a new form of the mathematical model of the CWU system is obtained. Based on Figs. 18-23, for small changes of variables $\Delta(\theta \cdot R)$, Δy and Δl_w one can write the following Eq.:

$$\Delta(\theta \cdot R) = -\Delta y - \Delta lw \tag{23}$$

Since the increment of the product $\Delta(\theta \cdot R)$ can be written in the following form:

$$\Delta(\theta \cdot R) = \Delta\theta \cdot R + \theta \cdot \Delta R \tag{24}$$

one can substitute Eq. (24) into Eq. (23) to obtain:

$$\Delta\theta \cdot R + \theta \cdot \Delta R = -\Delta y - \Delta lw \tag{25}$$

In this way, the relation between increments Δy, $\Delta\theta$, Δl_w, and ΔR is obtained.

One can see that the left side of Eq. (25), $\Delta\theta \cdot R+\theta \cdot \Delta R$, is dependent on increments $\Delta\theta$ and ΔR, because these variables are changeable during implementation of the task of CWU system.

If Eq. (25) is divided with a small increment of time Δt, in the limit one can write:

$$\dot{\theta} \cdot R + \theta \cdot \dot{R} = -\dot{y} - \dot{lw} \tag{26}$$

From Eq. (26) one can write the following equation for angular velocity of the winch:

$$\dot{\theta} = -\left(\dot{y}/R + \dot{lw}/R + (\theta \cdot \dot{R})/R\right) \tag{27}$$

From Eq. (27), one can see that angular velocity of θ is dependent on variables: θ and *R*, and velocity of *y*, *R* and l_w. Eq. (27) presents a kinematic relation between velocities of external *y* and internal coordinate θ and other dynamic variables.

The Kinematic Model of CWU System for Multi-row Radial and Axial CWU Process. Kinematic model of CWU system for multi-row radial and axial CWU process is defined with Eqs. (23)-(27). For regular winding/unwinding of the cable on the winch, this system has a translator motion of the winch along its axis z_w as well. This motion is labeled as c_θ. As it was previously described, this motion is usually implemented with the same motor as angular motion θ. For achieving the translator motion, this system consists of an additional gear. Relation between angular and translator motion was given in [34], and in case considered in this paper it is:

$$\theta = 2\pi \cdot c_\theta / d \tag{28}$$

In Eq. (28), variable d presents the diameter of the cable, see Figs. 21-23. It is assumed that the cable has an idealized circular cross-section.

Eq. (28) illustrates a linear relation between the angular and translator motion. After substituting Eq. (28) and its first derivative in Eq. (27), following equation for definition of translator velocity is achieved:

$$\dot{c}_\theta = \frac{-\frac{\dot{y}}{R}-\frac{l\dot{w}}{R}-\frac{\frac{2\pi}{d}\cdot c_\theta \cdot \dot{R}}{R}}{\frac{2\pi}{d}} = -\left((d \cdot \dot{y})/(2\pi \cdot R) + (d \cdot l\dot{w})/(2\pi \cdot R) + (c_\theta \cdot \dot{R})/R\right) \quad (29)$$

Eq. (29) shows that translator velocity of winch $\dot{c}_\theta$ along its axis z_w, depends on variables: c_θ, R, and d, and velocity of y, R and l_w. Eq. (29) presents another kinematic relation which is a result of Eq. (28). One can use either Eq. (27) or R and l_w are constant and their first derivatives are zero. One of these cases is shown in Fig. 22 and that is the period when only the first layer of cable is wound on the winch. In this case a simplified kinematic model is achieved from Eq. (27):

$$\dot{\theta} = -\dot{y}/R \quad (30)$$

In this case, kinematic model of translator motion in comparison to Eq. (29) is:

$$\dot{c}_\theta = -(d \cdot \dot{y})/(2\pi \cdot R) \quad (31)$$

Now, it is mathematically clear that application of only the first layer of cable winding/winding on the winch, shown in Fig. 22, is much simpler then application of cable winding/unwinding on the second, third or n-th layer on the winch, See Figs. 23 and 21.

The Dynamic Model of CWU System. In the previous sub-section, the equations which describe the kinematic model of CWU system have been defined. The kinematic model of this system presents a prerequisite for performing dynamic analysis of the CWU system. In order to define the dynamic model of CWU system one needs to identify the resultant torque which acts on shaft of the CWU system. Lagrange virtual work principle is used in this paper to acquire the following equation:

$$F \cdot \dot{y} = M \cdot \dot{\theta} \quad (32)$$

where F is the force acting on the load's weight m and M is the torque acting on the shaft of CWU system. By substituting Eq. (27) into Eq. (32), the following equation is obtained:

$$F \cdot \dot{y} = -M \cdot \left(\dot{y}/R + l\dot{w}/R + (\theta \cdot \dot{R})/R\right) \quad (33)$$

From Eq. (33), one can write the equation for resultant torque M:

$$M = -(F \cdot \dot{y})/\left(\dot{y}/R + l\dot{w}/R + (\theta \cdot \dot{R})/R\right) \quad (34)$$

Resultant torque M acting on the shaft of CWU system's winch includes the dynamics of the CWU process. It can be seen that the resultant torque M is dependent on geometry of the considered CWU system, Eqs. (32)–(34), i.e. it depends on variables: θ and R, and velocity of y, R and l_w.

Now the final form of the mathematical model of CWU system, which is analyzed in this paper, can be written. To define the dynamic model of CWU systems presented in Figs. 18-23, the well-known equation of motor will be used. The dynamic model of the CWU system is presented by

$$u = G_v \cdot \ddot{\theta} + L_v \cdot \dot{\theta} + S_v \cdot M \tag{35}$$

where: u – control signal (voltage) of the motor, G_v – motor's inertia characteristic, L_v – motor's damping characteristic, S_v – motor's geometric characteristics, while the first and the second derivatives of angular position θ of the winch, influence on the motor motion. Regardless that the motion of this system is influenced by velocity of R and l_w, the system does not get more complicated in the terms of number of DOFs.

*The Dynamic Model of CWU System for Multi-row Radial and Axial CWU Process***.** Dynamic model of CWU system for multi-row radial and axial CWU process is defined by Eqs. (32) – (35). These equations can be expressed through the winch's translator motion c_θ as well. If one substitutes the first derivative of Eq. (28) in Eq. (32), the following equation is determined:

$$F \cdot \dot{y} = M \cdot (2\pi \cdot \dot{c}_\theta)/d \tag{36}$$

By substituting Eq. (29) into Eq. (36), the following equation is obtained:

$$F \cdot \dot{y} = -M \cdot \big(\dot{y}/R + l\dot{w}/R + (2\pi \cdot c_\theta \cdot \dot{R})/(d \cdot R)\big) \tag{37}$$

From Eq. (37) one can express the resultant torque M in form:

$$M = -F \cdot \dot{y}/\big(\dot{y}/R + l\dot{w}/R + (2\pi \cdot c_\theta \cdot \dot{R})/(d \cdot R)\big) \tag{38}$$

Now the motor equation depending on the winch's translator motion c_θ can be written:

$$\mathrm{u} = \frac{2\pi}{\mathrm{d}} \cdot (\mathrm{G_v} \cdot \ddot{\mathrm{c}}_\theta + \mathrm{L_v} \cdot \dot{\mathrm{c}}_\theta)\text{-}\mathrm{S_v} \cdot \mathrm{F} \cdot \dot{\mathrm{y}}/\big(\dot{\mathrm{y}}/\mathrm{R} + \mathrm{l}\dot{\mathrm{w}}/\mathrm{R} + (2\pi \cdot \mathrm{c}_\theta \cdot \dot{\mathrm{R}})/(\mathrm{d} \cdot \mathrm{R})\big) \tag{39}$$

Special case of the mathematical model of CWU system for multi-row radial and axial CWU process is a period when dynamic variables R and l_w are constant and their first derivatives are zero. One of these cases is shown in Fig. 22 and that is the period when only first layer of cable is wound on the winch.

In this case, the load torque is:

$$M = -F \cdot R \tag{40}$$

Load torque from Eq. (40) can be achieved by using Eqs. (34) or (38).

The equations from this Section, define the general form of mathematical model of CWU system having variables R and l_w changeable during the motion of the load along line h.

In order to prove the validity of the mathematical formulations defined in this Section, in the following Section a novel program package, named CWUSOFT, is presented.

3.5. The Program Package CWUSOFT. Based on the mathematical model of CWU system, defined by Eqs. (23)–(40), a novel program package CWUSOFT has been synthesized. This program package contains several subroutines combined into one unit:

1. Subroutine for generation of the reference trajectory. In this case, the reference trajectory of the load in *x*-*y* space along the line *h* is defined. From *x*-*y* space, the internal coordinate, angular position of CWU system θ (as defined by Eq. (27)), is calculated. It should be noted that for CWU system for multi-row radial and axial CWU process it is possible to calculate the translator motion c_θ of the winch as well. This procedure includes the kinematic model of the CWU system.
2. Subroutine for generation of the dynamic response of the CWU system. In this subroutine, the influence of the changes of radius *R* and length between the winch and hanging point *lw* is included. This is defined through the resultant torque *M* which includes the dynamics of load's motion (force *F*) via Lagrange virtual work principle. Eq. (34) includes the geometry of the mechanism, i.e. its kinematic model, as well. It can be seen that now the relation between the resultant torque *M* and force *F* is related via the following variables: θ and *R*, and velocity of *y*, *R* and l_w. It should be emphasized that for CWU system for multi-row radial and axial CWU process one can use the Eq. (38) as well.
3. Subroutine for control structure of the system. This routine assumes the creation of various control algorithms for the motion control of the load in *x*-*y* space along the line *h*.

Based on the analysis from Sections 3, next part of the paper will show the simulation results which illustrate the implementation of one trajectory of one type of the CWU system.

3.6. Testing the CWU System – Simulation Results. In this Section one example of CWU system's load motion is simulated. CWU system named system for smooth single – row radial multi-layered CWU process from Figs. 19b and 20 was chosen.

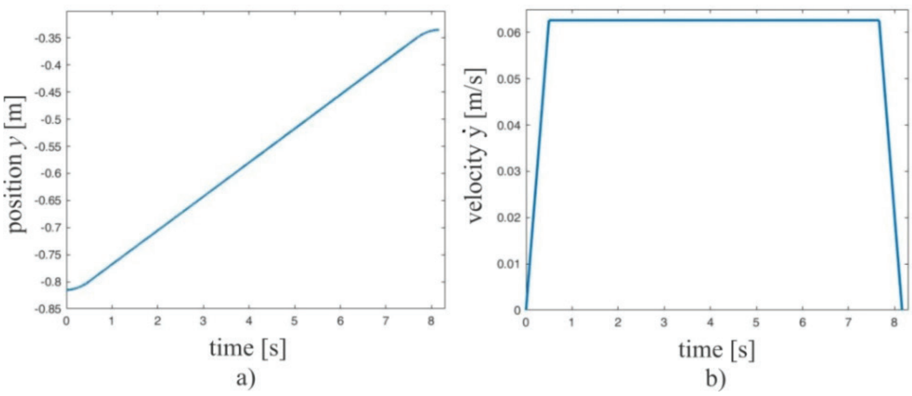

FIGURE 24. a) position and b) velocity of load's motion.

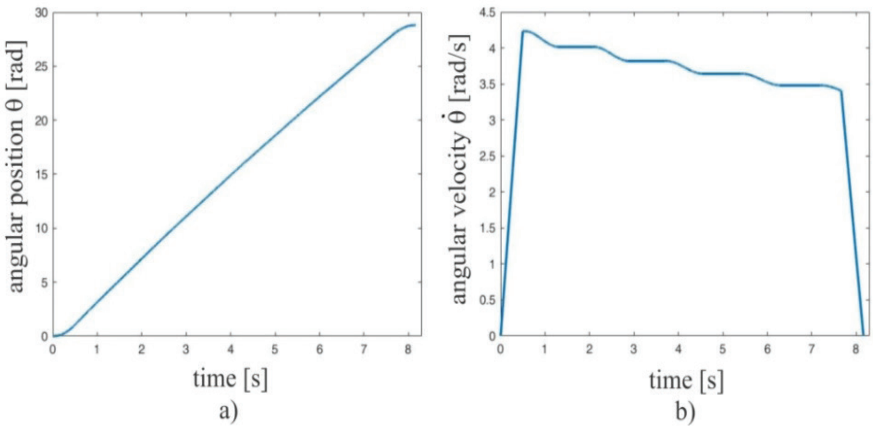

FIGURE 25. Angular a) position θ and b) velocity of CWU system.

This system has constructive radii: R_{i0}*=0.0136(m)* and $R_{i0(withtilde)}$*=0.014(m)* . The mathematical model of CWU system defined in Section 3.4 will be tested. For generation of all the results in this Section, the program package CWUSOFT from Section 3.5 is used. The considered CWU system has the carrying capacity of *0.064(kg)*.

For the purpose of testing, the following reference trajectory has been used: the load needs to move along the line *h* from point y_{start}*=-0.815(m)* to point y_{end}*=-0.335(m)*. Total load carrying length is *0.48(m)*. See Fig. 24a. During the load lifting, cable is wound on the winch. Velocity of the load has a trapezoidal shape with maximal value of *0.063(m/s)*. See Fig. 24b. For driving the winch, a DC motor with rated voltage of *12(V)* was used.

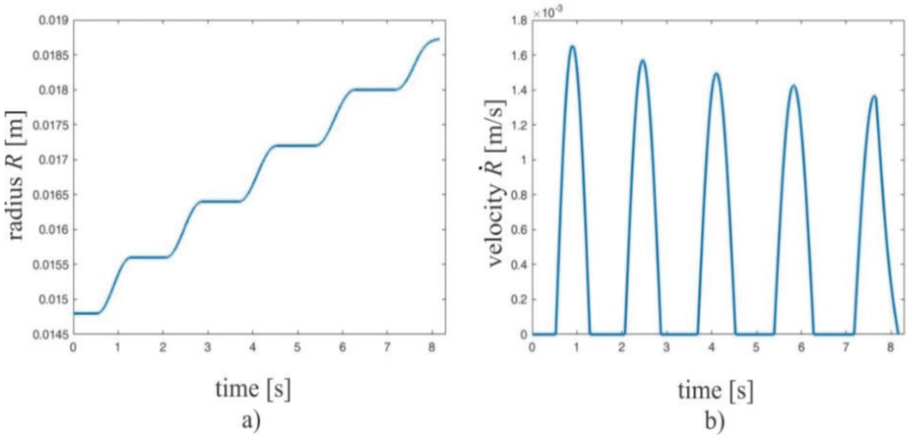

FIGURE 26. a) Winding/unwinding radius R and b) its velocity.

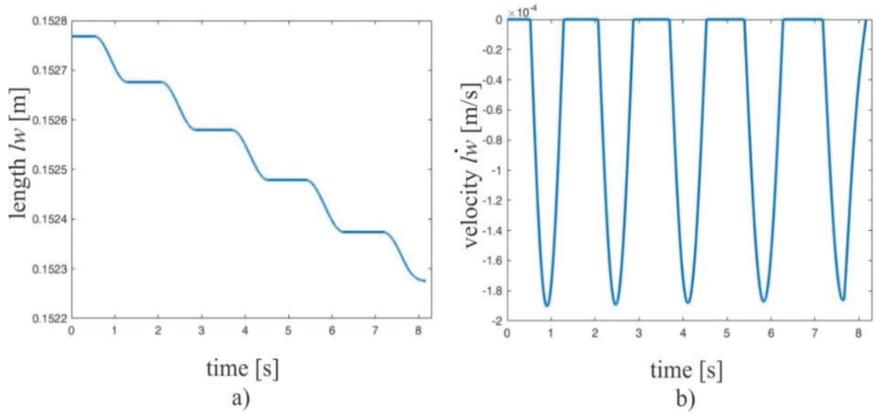

FIGURE 27. a) Length l_w and b) its velocity.

By using Eq. (27) and based on the geometry of examined CWU system, angular velocity of θ of the CWU system is determined and that is shown in Fig. 25b. By integrating this variable, angular position of CWU system is achieved, see Fig. 25a. Total angular motion of the CWU system during the task execution is from *0* to *28.82(rad).* Maximal angular velocity is *4.235(rad/s).*

Fig. 26a shows the change of winding/unwinding radius *R* during the task implementation, while Fig. 26b shows its velocity. At the beginning, from *0 – 0.48(s)*, the CWU system is winding inside the *con* area, where its radius *R* has a constant value of *R=0.0148(m)*, while its first derivative is *=0*. After this moment, from *0.48 – 1.26(s)*, the CWU system is inside the *smvar* area and during this period of time radius *R* grows and its first derivative is *>0*. As it can be seen from Fig. 26, during the load lifting, i.e. during the cable winding on a winch, a cyclical alternation of *con* and *smvar* areas occurs. This statement is confirmed by Fig. 26b where one can see the change of velocity of *R* during the load lifting. As radius *R* changes its value during the load lifting, length l_w and angle γ change their values as well.

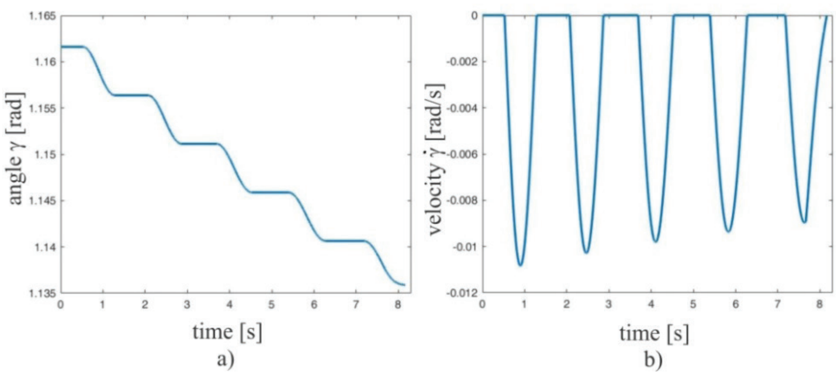

FIGURE 28. a) Angle γ and b) its velocity.

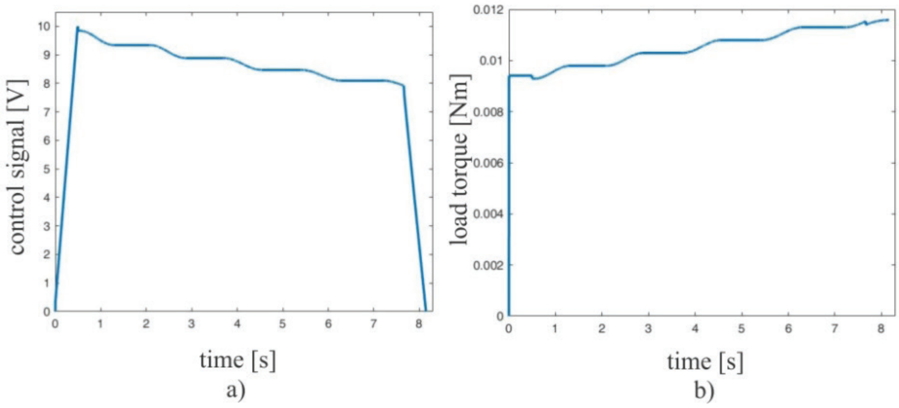

FIGURE 29. Control signal u and b) load torque M.

Fig. 27a shows the change of the length l_w, while Fig. 27b shows the first derivative of this variable $\dot{l}_w$. From these figures one can see that this variable has a smooth change in time. By comparing the Figs. 27a and 26a, one can see that during the *con* period both R and l_w are constant. Unlike the *con* period, when winch is in the *smvar* period during the cable winding, radius R is growing while length l_w is decreasing in the same period.

In Fig. 28a, change of the angle γ during the load lifting is presented, while Fig. 28b shows its first derivative $\dot{\gamma}$. From these figures, one can see that angle γ has the same change dynamics as length l_w - when cable is winding both l_w and γ decrease their values. When winch is in the *con* area, i.e. when *R=const*, angle γ also has a constant value, as well as length l_w.

Fig. 29a presents the control signal *u,* while Fig. 29b shows the load torque M which acts on the CWU system's shaft. One can see that the load toque is growing during the cable winding and that is due to the growth of radius R during the task implementation.

In this part of the paper, simulation results which show load lifting process were shown. During the load lifting process, cable is always winding on the winch. Opposite process of cable unwinding was not shown, because all the phenomena that occur during the process of winding occur during the process of unwinding as well only in opposite direction.

Next Section of the paper will present an experimental analysis which will confirm theoretical results from 3.4 Section and simulation results from 3.6 Section of the paper.

3.7. Experimental Results. In this part of the paper, experimental confirmation of simulation and theoretical results from previous Sections will be given.
Experiment was made on the set-up shown in Fig. 30.

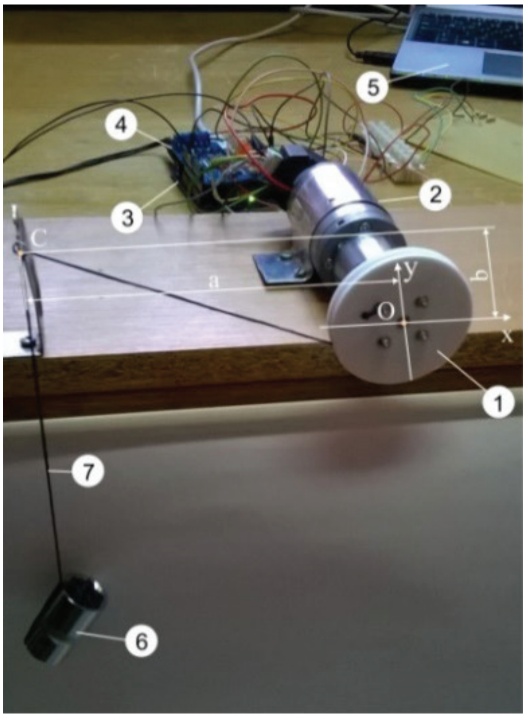

FIGURE 30. The experimental set-up.

The winch is in Fig. 30 labeled as position 1. The following components have been used: DC motor, 12V, 20W with encoder and gear head (position 2), Arduino UNO REV3 (position 3), Arduino Motor Shield REV3 (position 4) and a laptop computer (position 5). The mass of the load (position 6) which is lifted is 0.064 kg, while the total cable (position 7) winding length is 0.48 m, lengths a and b are a=0.147 m, b=0.045 m. Duration of the motion is 8.2 s. Experiment was made on a CWU system which uses a winch from Fig. 19b whose constructive radii are: R_{i0}*=0.0136(m)* and $R_{i0(withtilde)}$*=0.014(m)*. All the parameters are the same as ones used for simulation results. Because of that, experimental and simulation results are comparable.

Fig. 31a shows angular position of the CWU system during the task implementation. This figure presents results achieved by simulations θ and experiment θ_{exp}. One can see that θ_{exp} has a change from *0* to *27.3(rad)*, while θ has a change from *0* to *28.82(rad).* It is clear that θ_{exp} can never achieve the value of θ, because of the problem of un-modeled frictions in CWU system. Fig. 31b presents comparison between angular velocities of θ of the CWU system achieved with simulation and experiment. In general, it can be said that angular velocity has decrease of value during the task execution which is caused by the growth of load torque acting on the CWU system's shaft. By comparing simulation and experiment angular velocities of θ, one can also conclude that because of unmodeled frictions experiment angular velocity on average always has a value which is under simulation angular velocity (average value). This causes $\theta_{exp} < \theta$ for each moment during the task execution.

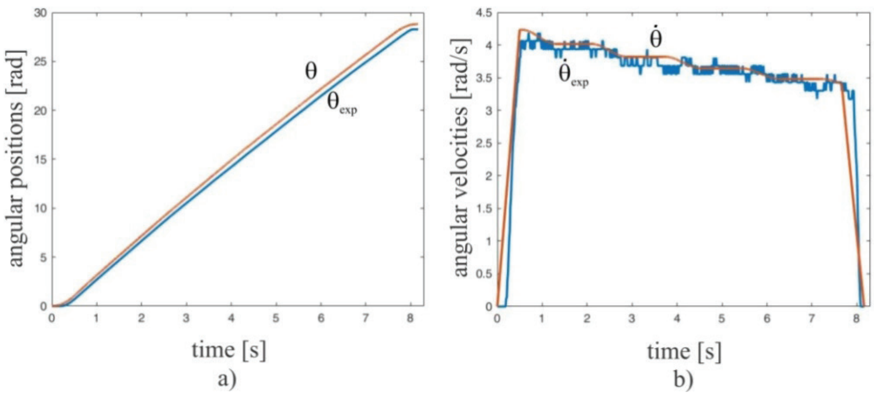

FIGURE 31. Angular a) position and b) velocity of the CWU system.

4. Concluding Remarks

Six types of CPR systems: RSCPR, RFCPR, CPR-A, CPR-B, CPR-C, and CPR-D system, are presented, modeled and analyzed.

The geometric relations between the motor and the camera motion are highly important for the kinematic and dynamic modeling of each system.

The relation between internal and external coordinates is described by the Jacobian matrix J. This methodology for developing the kinematic model of selected systems is named the KinCPR-Solver (Kinematic Cable Parallel Robot Solver), and it gives a precise direct and inverse kinematic solutions.

The relation between the forces in the ropes and the forces acting at the camera carrier cannot be solved by using the original form of Lagrange's principle of virtual work. Because of the CPR system complexity, the Lagrange's principle of virtual work has been adapted and changed. This equation has been used for determining the dynamic model of the CPR system. This calculation shows the influence of the external forces on the motor dynamics. The motors' mathematical models are defined in classical form.

The Jacobian matrix J and moment mapping matrix O for each system are significantly different, which is the consequence of their different constructions.

For the four case studies, the software packages: AIRCAMA, AIRCAMB, AIRCAMC, and AIRCAMD, have been developed to analyze the CPR-A, CPR-B, CPR-C, and CPR-D models, respectively, under same conditions.

Oscillatory character of the responses presented on Fig. 14-17. Compare simulation results for all four constructions, CPR-A, CPR-B, CPR-C, and CPR-D, mutually.

By the comparative analysis of the results, we can come to the conclusion that these four CPR constructions follow the same trajectory of the camera carrier. It is important to notice that every construction has totally different motion of motors for the same camera trajectory. Analyzing the results of these four CPR constructions responses indicates their differences.

The general mathematical model of cable winding/unwinding (CWU) system is presented. CWU system includes motor, gear and the winch, and it is one of main parts of any CPR system. This model is defined in general form for CWU systems from Figs. 19-23.

The purpose of this research is pointing out the complexity of CWU systems. Even at these simple constructions shown in Figs. 19-23 where each of them contains motor, gear and winch one can see the influence of winding radius R and length l_w on system's dynamics of response.

For the verification of the defined mathematical model, a novel program package CWUSOFT was defined. Simulation results are shown through relevant dynamic variables of CWU system: angular position θ, radius R, length l_w and angle γ. Simulation results were performed for one novel type of CWU system, see Figs. 19b and 20. Simulation results were achieved by using the program package CWUSOFT. These simulation results as well as theoretical definitions were confirmed through the experimental analysis.

CWU systems can be sub-systems of more complex mechatronic systems and in that case the mathematical model of this complex system is much more complicated and one of the reasons is mutual coupling of several CWU sub-systems. Because of that, it is very important that dynamic characteristics which are indicated in this paper are included in the analysis and synthesis of these complex mechatronic systems. This will be a subject of future research of authors of this paper.

Acknowledgments
This research was supported by the Ministry of Education, Science and Technological Development, Government of the Republic of Serbia: Grant OI-174001 and "The dynamics of hybrid systems of complex structure", by Institute SANU Belgrade and Faculty of Mechanical Engineering University of Nis, Serbia, Grant TR-35003 through the following two projects: "Ambientally intelligent service robots of anthropomorphic characteristics", by Mihailo Pupin Institute, University of Belgrade, Serbia. We are grateful to Prof. Dr. Katica R. (Stevanovic) Hedrih from Mathematical Institute, Belgrade for helpful consultations during this research and we are grateful to our former colleague Zivko Stikic for his help during this research.

References

[1] C. Gosselin, J. Angeles, *The Optimum Kinematic Design of a Planar Three-Degree-of-Freedom Parallel Manipulator*, Journal of Mechanisms, Transmissions, and Automation in Design **110** (1988), 35-41.

[2] J. Fang, Z. Huang, *Kinematics of a three-degree-of-freedom in-parallel actuated manipulator mechanism*. Mech. Mach. Theory **32** (1997), 789-796.

[3] P.H. Borgstrom, N.P. Borgstrom, M.J. Stealey, B. Jordan, G. Sukhatme, M.A. Batalin, W. J. Kaiser, *Discrete Trajectory Control Algorithms for NIMS3D, an Autonomous Underconstrained Three-Dimensional Cabled Robot*, Proceedings of the 2007 IEEE/RSJ *International Conference on Intelligent Robots and Systems*, San Diego, CA, USA, 2007.

[4] J.P. Merlet, *MARIONET*, *A Family of Modular Wire-Driven Parallel Robots*, Advances in Robot Kinematics: Motion in Man and Machine **1** (2010), 53-61.

[5] M. Gouttefarde, J.P. Merlet, D. Daney, *Determination of the wrench-closure workspace of 6-DOF parallel cable-driven mechanisms*, Advances in Robot Kinematics **5** (2006), 315-322.

[6] T. Bruckmann, L. Mikelsons, D. Schramm, M. Hiller, *Continuous workspace analysis for parallel cable-driven Stewart-Gough platforms*, Special Issue: Sixth International Congress on Industrial Applied Mathematics (ICIAM07) and GAMM Annual Meeting, Zürich 7, 2007.

[7] A. Pott, *Forward Kinematics and Workspace Determination of a Wire Robot for Industrial Applications*, Advances in Robot Kinematics: Analysis and Design **7** (2008), 451-458.

[8] P. Miermeister, A. Pott, A. Verl, *Auto-Calibration Method for Overconstrained Cable-Driven Parallel Robots*, ROBOTIK *7th German Conference on Robotics*, Munich, Germany, 2012.

[9] T. Higuchi, A. Ming, J. Jiang-Yu, *Application of multi-dimensional wire crane in construction*, In *5th Int. Symp. on Robotics in Construction*, Tokyo, 661–668, 1988.

[10] M. Filipovic, A. Djuric, Lj. Kevac, *The rigid S-type cable-suspended parallel robot design, modelling and analysis*, Robotica **34**(9) (2016), 1948-1960.

[11] M. Filipovic, *Comparative analysis of two types of Cable-suspended Parallel Robots, RSCPR system and RFCPR system*, *International Symposium INFOTEH-JAHORINA*, Bosnia and Herzegovina **13**, 1057-1062, 19-21 March 2014.

[12] M. Filipovic, A. Djuric, Lj. Kevac, The *significance of adopted Lagrange principle of virtual work used for modeling aerial robots*, Applied Mathematical Modelling **39**(7) (2015), 1804-1822.

[13] M. Filipovic, A. Djuric, *Mathematical Model of the Aerial Robotic Camera base on its Geometric Relationship*, FME Transactions, Scientific journal, Faculty of Mechanical Engineering, Belgrade, Serbia **42**(2) (2014), 133-141.

[14] M. Filipovic, A. Djuric, *Cable-suspended CPR-D type parallel robot*, Journal of Theoretical and Applied Mechanics, Poland, J THEOR APP MECH-POL, Warsaw **54**(2) (2016), 645-657.

[15] Lj. Kevac, M. Filipovic, A. Rakic, *The trajectory generation algorithm for the cable-suspended parallel robot – the CPR trajectory solver*", Robotics and Autonomous Systems, Elsevier **94** (2017), 25-33.

[16] Lj. Kevac, M. Filipovic, A. Rakic, *Contribution to modelling the cable-suspended parallel robot intended for application in greenhouses*, International Journal of Robotics and Automation **33**(2) (2018), 194-201.

[17] M. Filipovic, Lj. Kevac, *A novel methodology for choosing actuators of Cable-suspended parallel robots*, Scientific Journal FACTA UNIVERSITATIS, Series: Automatic Control and Robotics **17**(2) (2018), 71-91.

[18] Lj. Kevac, Z. Stikic, M. Filipovic, *Multivariable procedure for definition of CPR system's feasible workspace*, Engineering & Automation Problems, International Journal, Moscow Centre for Scientific and Technical Information **2** (2019), 76-89.

[19] Lj. Kevac, M. Filipovic, A. Djuric, *Mathematical model of the artificial muscle with two actuators*, Proceedings of the Institution of Mechanical Engineers, Part C: Journal of Mechanical Engineering Science, Institution of Mechanical Engineers (2020), 1-16. DOI: 10.1177/0954406220941565

[20] J.V. Zietzwitz, L. Fehlberg, T. Bruckmann, H. Vallery, *Use of passively guided deflection units and energy-storing elements to increase the application range of wire robots*, Proceedings of *First International Conference on Cable-Driven Parallel Robots,* Stuttgart, Germany, 2012.

[21] United Nations, *Cable Logging Systems,* Food and agriculture organization of the united nations, Roma, Italy, 1981.

[22] I. Samset, *Winch and cable systems (Forestry Sciences)*, Springer-Verlag GmbH, Berlin, Germany, 1985.

[23] E.M. Abdel-Rahman, A.H. Nayfeh, Z.N. Masoud, *Dynamics and Control of Cranes, A Review*, Journal of Vibration and Control **9** (2003), 863-908.

[24] D.G. Padfield, *The motion and tension of an unwinding thread*, Proceedings of the Royal Society, Londond, UK, 1956.

[25] W.B. Fraser, T.K. Ghosh, S.K. Batra, *On Unwinding Yarn from a Cylindrical Package*, Proceedings of the Royal Society, Londond, UK, 9 March 1992.

[26] J.D. Clark, W.B. Fraser, D.M.Stump, *Modelling of tension in yarn package unwinding*, Journal of Engineering Mathematics **40** (2001), 59–75.
[27] E. Imanishi, T. Nanjo, T. Kobayashi, *Dynamic simulation of wire cable with contact*, Journal of Mechanical Science and Technology **23** (2009)**,** 1083-1088.
[28] M. Szczotka, S. Wojciech, A. Maczynski, *Mathematical model of a pipelay spread*, The Archive of Mechanical Engineerin **54** (2007), 27-46.
[29] J.W. Lee, K.W. Kim, H.R. Kim, W.S. Yoo, *Prediction of un-winding behaviors and problems of cables from inner-winding spool dispensers*, Nonlinear Dynamics **67** (2012)**,** 1791–1809.
[30] Lj. Kevac, M. Filipovic, A. Rakic, *Dynamics of the process of the rope winding (unwinding) on the winch*, Applied Mathematical Modelling, Elsevier **48** (2017), 821-843.
[31] Lj. Kevac, M. Filipovic, Z. Stikic, Registered patent at the national level, Owner: Mihailo Pupin Institute, *A winch with profiled drum section for smooth single rowed multilayered radial winding of the rope*, IPC B66D 1/30; B66D 1/36, Application number П-2015/0598, Publication date of application (A1) 31.03.2017, number of gazette 3/2017, Registration number 57921 B1, Number of decision to grant the right 2018/18117, date of publication of the patent 31.01.2019, The Intellectual Property Office, Republic of Serbia, 2018.
[32] M. Filipovic, Lj. Kevac, *A new Winch Construction for Smooth Cable Winding/Unwinding*, Scientific Journal FACTA UNIVERSITATIS, Series: Mechanical Engineering, University of Niš **15**(3) (2017), 367 – 381.
[33] Lj. Kevac, M. Filipovic, *Mathematical Model of Cable Winding/Unwinding System*, Journal of Mechanics, J MECH, Cambridge University press, (2017), 1-13.
[34] E.D. Ruiz-Rojas, J.L. Vazquez-Gonzalez, R. Alejos-Palomares, A.Z. Escudero-Uribe, J.R. Mendoza-Vázquez, *Mathematical Model of a Linear Electric Actuator with Prosthesis Applications*, Proceedings of *18th International Conference on Electronics, Communications and Computers*, CONIELECOMP 2008, Cholula, Puebla, Mexico, 2008.